REVIEW

Check for updates

Proton conductive Zr-based MOFs

Xin Chen and Gang Li (iD) *

The applications of crystalline solid-state proton conductive materials in fuel cells, proton sieving, electrochemical sensing and biochemistry are in the foreground, among which proton conducting metal–organic frameworks are favored by researchers for their structural diversity, functional design and modification. As one class of promising candidates for proton conductors, Zr-based metal–organic frameworks (MOFs) have attracted considerable attention. Therefore, the proton conductivity of such complexes will be comprehensively summarized for the first time by us. Herein, the proton conductivity properties of these MOFs with ordered porous structures, outstanding thermal stability, remarkably high water stability and chemical stability will be reviewed. These MOFs are classified and summarized according to the types of constructed organic ligands, such as carboxylic, phosphoric, and nitrogenous ligands. Consequently, the preparation strategy, structural characteristics, proton conductivity, conduction mechanism and application value are discussed. Finally, based on our experimental experience and literature review, the future development direction and application of this type of proton conducting MOF are assessed and highlighted.

1. Introduction

In today's world, with the rapid development of global industry and the improvement of people's living standards, global energy consumption continues to reach an unprecedented level, which leads to the rapid consumption of fossil fuels such as oil and natural gas. The resulting energy crisis and environmental pollution have become two major problems that must be solved. To solve these two problems, people hope to use more clean energy sources or new alternative energy such as fuel cells (FCs).[1] In this context, proton exchange

College of Chemistry and Green Catalysis Center, Zhengzhou University, Zhengzhou 450001, Henan, P. R. China. E-mail: gangli@zzu.edu.cn

Xin Chen obtained her B.S. degree in chemistry from Anyang Normal University, in 2019. She is currently pursuing an M.Sc. Program under the guidance of Prof. Gang Li at Zhengzhou University. Her research interests are the design of functional solid crystalline materials and their application in the field of proton conductivity.

Xin Chen
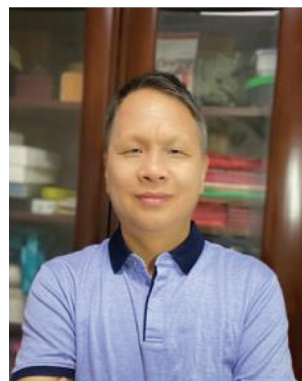
Gang Li received his B.S. degree and M.S. degree in inorganic chemistry from Zhengzhou University, China. He obtained his Ph.D degree in 2003 from Shanxi University, China. Then he joined the Zhengzhou University. From January to July in 2004, he worked at the Chinese University of Hongkong as a Visiting-Scholar. Then he did his reasearch at the University of Sussex as a post-doctoral researcher from

Gang Li

September, 2004 to September, 2005. He became a professor in Chemistry at the Zhengzhou University in 2008. His main research interest is focused on the design of various functional solid crystalline materials (MOFs, COFs and HOFs) to develop their applications in the field of energy and identification.

This journal is © the Partner Organisations 2020

Inorg. Chem. Front., 2020, **7**, 3765–3784 | **3765**

membrane fuel cells (PEMFCs) are favoured by many researchers for their advantages of efficient energy conversion and nearly zero emission and so on.[2] In PEMFCs, a proton exchange membrane (PEM) provides a channel for proton transport, making protons pass across the film from the anode to the cathode, and forming a circuit with the electron transfer in the external circuit to provide current to the outside world. Therefore, the performance of PEMs plays a very important role in the performance of PEMFCs. As one core component, the PEM directly determines the service life and performance of PEMFCs. Therefore, the design, preparation and development of proton exchange membranes with outstanding performance have attracted much attention.[2–5]
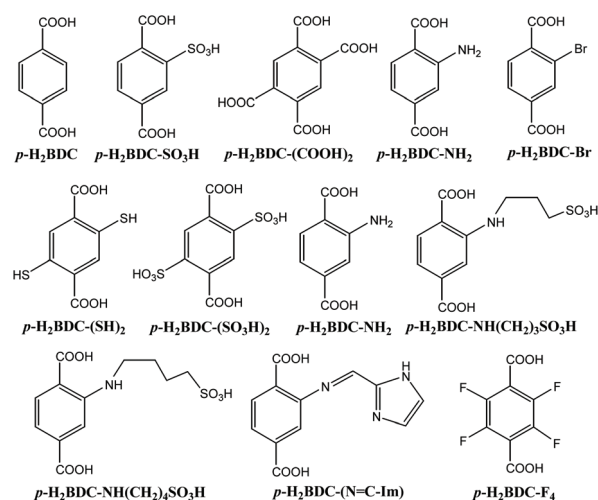
To date, the most commonly used PEM is the Nafion series perfluorinated sulfonic acid membrane with high proton conductivity (σ) and good chemical stability. Nevertheless, such a membrane has the following disadvantages: (1) it is very difficult to synthesize and sulfonate perfluorinated substances, which makes the film formation difficult and leads to high costs; (2) requirements of high temperature and H_2O content. The optimal operating temperature of Nafion series films is 70–90 °C; exceeding this temperature range will cause a sharp decrease in water content and a rapid decline in electrical conductivity; (3) some hydrocarbons, such as methanol (MeOH), have high permeability and are not suitable for use as PEMs in direct methanol fuel cells (DMFC). (4) The poor crystalline structural characteristics of such membranes make it impossible to deeply analyse and study the proton conductive mechanism, which limits the demand for improving the proton conductivity.[6,7] Therefore, the development of new and inexpensive proton-conducting materials with excellent performance has been a subject of intensive research.

Recently, the research of an important family of crystalline solid materials, such as metal–organic frameworks (MOFs),[8–20] covalent organic frameworks (COFs),[21–24] and hydrogen-bonded organic frameworks (HOFs)[25–30] acting as promising conductors has attracted great attention. In addition to the structural modifying ability and functional modulability of such crystalline materials, which are well known to us, they also have high crystallinity, which provides a good material basis for the in-depth study of the proton conduction mechanism.

Here we will focus on the proton conducting properties of MOFs with ordered structures, which are assembled by metal ions or clusters with bridging organic ligands. Since a 2D copper(II) MOF, [(HOC_2H_4)_2-dtoa-Cu] (dtoa = dithiooxamide) with proton conductivity was reported for the first time in 1979,[31] a great number of studies have been conducted on proton conductive MOFs, especially in recent years. Through a large number of explorations, it has been found that MOFs can be a good candidate for proton conductors for the following reasons: first, the porous structures of MOFs contain rich H-bonds and water clusters, which can carry out proton transmission quickly and efficiently; second, the single crystal products of MOFs are relatively easy to

obtain, and their fine structural characteristics can be obtained through X-ray crystallography, which provides convenience for the exploration of the proton conduction mechanism; third, the proton conductivity of MOFs can be tuned by selecting different metal ions or modifying multifunctional organic ligands or the post-modification method. Although the research on the proton conductivity of such MOFs has been summarized and evaluated by several groups covering phosphate MOFs,[32] carboxylate MOFs,[33] and so on,[34–39] most of these reviews are broad and do not include specific reviews of MOFs of a certain metal atom, especially zirconium-based MOFs. It has been found in past studies that a significant number of proton conducting MOFs are of low stability, which limits their further practical application.[33] Therefore, it is one of the preconditions to search for MOFs with ultrahigh structural and chemical stability for proton conductivity research.

Since the Cavka group first reported a terephthalic zirconium MOF, **UiO-66** (UiO = University of Oslo) in 2008,[40] there is great interest in this class of MOFs with superior water stability and chemical stability. After twelve years of research and exploration, people have carried out in-depth studies on various properties of Zr-based MOFs including UiO series, PCN series, NU series and DUT series.[41–43] Nevertheless, until now, there has not been a systematic and comprehensive review of the research of these MOFs in the field of proton conductivity, although there have been many recent exciting research developments. In this review, we will summarize the design strategy, structural characteristics, proton conductivity and proton conduction mechanism of such MOFs, and look forward to the future development trend. We hope that this review will enable us to design and prepare novel proton-conductive zirconium-based MOFs more efficiently and quickly for future applications. Scheme 1 gives the organic linkages appearing in the UiO series MOFs. Table 1 lists the proton conducting Zr-based MOFs described so far.

Scheme 1 The organic linkages appearing in the **UiO-66** series MOFs.

3766 | *Inorg. Chem. Front.*, 2020, **7**, 3765–3784

This journal is © the Partner Organisations 2020

Table 1 Proton conduction in Zr-based MOFs and related composite membranes

Organic linkages	MOFs	Structures	Syntheses	σ/S cm^{-1}	E_a/eV	Ref.
$p\text{-}H_2BDC$	$Zr_6O_4(OH)_{4.6}(p\text{-}BDC)_{5.7}$	3D	Ligand defect control method	1.30×10^{-5} (65 °C, 95% RH)	0.25	44
$p\text{-}H_2BDC$	$Zr_6O_4(OH)_{5.6}(p\text{-}BDC)_{5.2}$	3D	Ligand defect control method	6.61×10^{-5} (65 °C, 95% RH)	0.29	44
$p\text{-}H_2BDC$	$Zr_6O_4(OH)_{6.8}(p\text{-}BDC)_{4.6}$	3D	Ligand defect control method	1.01×10^{-3} (65 °C, 95% RH)	0.36	44
$p\text{-}H_2BDC$	$Zr_6O_4(OH)_4(p\text{-}BDC)_{5.3}(O_2CCH_3)_{1.4}$	3D	Ligand defect control method	2.75×10^{-5} (65 °C, 95% RH)	0.29	44
$p\text{-}H_2BDC$	$Zr_6O_4(OH)_{4.8}(p\text{-}BDC)_{5.6}$	3D	Ligand defect control method	2.63×10^{-4} (65 °C, 95% RH)	0.32	44
$p\text{-}H_2BDC$	$Zr_6O_4(OH)_6(p\text{-}BDC)_5$	3D	Ligand defect control method	6.93×10^{-3} (65 °C, 95% RH)	0.22	44
$p\text{-}H_2BDC\text{-}SO_3H$	$Zr_6O_4(OH)_8(p\text{-}BDC\text{-}SO_3H)_{4.2}\cdot 67H_2O$	3D	Solution reaction	1.93×10^{-3} (65 °C, 95% RH)	0.25	45
$p\text{-}H_2BDC\text{-}SO_3H$	$Zr_6O_4(OH)_8(p\text{-}BDC\text{-}SO_3H)_4\cdot 65H_2O$	3D	Solution reaction	2.40×10^{-3} (65 °C, 95% RH)	0.25	45
$p\text{-}H_2BDC\text{-}SO_3H$	$Zr_6O_4(OH)_8(p\text{-}BDC\text{-}SO_3H)_4\cdot 80H_2O$	3D	Solution reaction	5.62×10^{-3} (65 °C, 95% RH)	0.24	45
$p\text{-}H_2BDC\text{-}SO_3H$	$Zr_6O_4(OH)_8(p\text{-}BDC\text{-}SO_3H)_{3.8}\cdot 153H_2O$	3D	Post-modified method	3.46×10^{-3} (65 °C, 95% RH)	0.25	45
$p\text{-}H_2BDC\text{-}(COOH)_2$	UiO-66-SO$_3$H	3D	Solvothermal synthesis	3.4×10^{-3} (30 °C, ~97% RH)	0.27	50
$p\text{-}H_2BDC\text{-}(COOH)_2$	UiO-66-2COOH	3D	Solution reaction	1.0×10^{-3} (30 °C, ~97% RH)	0.18	50
$p\text{-}H_2BDC\text{-}NH_2$	UiO-66-NH$_2$	3D	Solvothermal synthesis	1.40×10^{-5} (30 °C, ~97% RH)	0.40	50
$p\text{-}H_2BDC$	UiO-66	3D	Solvothermal synthesis	7.54×10^{-6} (30 °C, ~97% RH)	0.44	50
$p\text{-}H_2BDC\text{-}Br$	UiO-66-Br	3D	Solvothermal synthesis	2.23×10^{-7} (30 °C, ~97% RH)	0.78	50
$p\text{-}H_2BDC$	UiO-66	3D	Solvothermal synthesis	2.5×10^{-5} (80 °C, 90% RH)	–	51
$p\text{-}H_2BDC\text{-}(SH)_2$	UiO-66(SH)$_2$	3D	Micarowave reaction	4.3×10^{-6} (80 °C, 90% RH)	0.23	51
$p\text{-}H_2BDC\text{-}(SO_3H)_2$	UiO-66(SO$_3$H)$_2$	3D	Post-synthetic oxidation	8.4×10^{-2} (80 °C, 90% RH)	0.32	51
$p\text{-}H_2BDC\text{-}F_4$	UiO-66-F$_4$	3D	Solution reaction	—	—	52
$p\text{-}H_2BDC\text{-}NH(CH_2)_3SO_3H$	PSM 1	3D	Post-synthetic modification	1.64×10^{-1} (80 °C, 90% RH)	0.107	53
$p\text{-}H_2BDC\text{-}NH(CH_2)_4SO_3H$	PSM 2	3D	Post-synthetic modification	4.66×10^{-3} (80 °C, 90% RH)	0.292	53
$p\text{-}H_2BDC\text{-}NH_2$	UiO-66-NH$_2$	3D	Solvothermal synthesis	3×10^{-6} (80 °C, 98% RH)	—	54
$p\text{-}H_2BDC\text{-}NH_2 + p\text{-}H_2BDC\text{-}SO_3H$	UiO-66-AS	3D	Post-synthetic modification	1.7×10^{-4} (80 °C, 98% RH)	0.2	54
$p\text{-}H_2BDC\text{-}SO_3H + p\text{-}H_2BDC\text{-}(N{=}C\text{-}Im)$	IM-UiO-66-AS	3D	Solution-casting method	1.54×10^{-1} (80 °C, 98% RH)	0.32	54
	IM-UiO-66-AS@PP (60 wt%)	Film	Solution-casting method	1.19×10^{-2} (80 °C, 98% RH)	0.32	54
$p\text{-}H_2BDC\text{-}(COOH)_2$	UiO-66-2COOH	3D	Solution reaction	2.3×10^{-3} (90 °C, 95% RH)	0.17	56
$p\text{-}H_2BDC\text{-}NH_2$	UiO-66-NH$_2$ + UiO-66-SO$_3$H/Nafion-0.6	Film	Solution-casting method	0.256 (90 °C, 95% RH)	—	57
$p\text{-}H_2BDC\text{-}SO_3H$	CS/UiO-66-SO$_3$H-6	Film	Solution-casting method	1.52×10^{-3} (90 °C, anhydrous)	0.105	58
$p\text{-}H_2BDC\text{-}NH_2$	UiO-66-NH$_2$-15	Film	Solution-casting method	0.0564 (100 °C, 98% RH)	0.12	58
$p\text{-}H_2BDC\text{-}NH_2$	CS/UiO-66-SO$_3$H-6 + UiO-66-NH$_2$-15	Film	Solution-casting method	5.2×10^{-2} (100 °C, 98% RH)	0.131	58
$p\text{-}H_2BDC\text{-}SO_3H$	GO@UiO-66-NH$_2$/Nafion-0.6	Film	Solution-casting method	3.78×10^{-3} (120 °C, anhydrous); 0.303 (90 °C, 95% RH)	0.189	59
$p\text{-}H_2BDC\text{-}NH_2$	SPEN/UiO-66-NH$_2$-5	Film	Solution-casting method	3.403×10^{-3} (90 °C, anhydrous); 1.351×10^{-1} (80 °C, hydrated in H$_2$O)	—	60
$p\text{-}H_2BDC\text{-}NH_2$	UiO-66-NH$_2$@NFs/Nafion	Film	Impregnating method	0.27 (80 °C, 100% RH)	—	61
$p\text{-}H_2BDC\text{-}SO_3H$	SPEEK/UiO-66-SO$_3$H@GO-10	Film	Solution-casting method	0.268 (70 °C and 95% RH)	—	62
$p\text{-}H_2BDC$	UiO-66(200)/Nafion-2	Film	Solution-casting method	0.207 (110 °C and 95% RH)	—	63
$p\text{-}H_2BDC\text{-}SO_3H$	UiO-66-SO$_3$H/Nafion-2	Film	Solution-casting method	0.189(110 °C and 95% RH)	—	63
$p\text{-}H_2BDC\text{-}SO_3H$	BSP/Zr-Cr-SO$_3$H-0.5%	Film	Solvothermal synthesis	0.154 (80 °C and 100% RH)	—	64
H_2bpdc	Him@UiO-67	3D	Evaporation method	1.52×10^{-3} (130 °C, anhydrous)	0.36	65
$H_2bpdc\text{-}4SO_2Me4F$	Zr-bpdc-4SO$_2$Me4F	3D	Oxidation method	1.75×10^{-3} (100 °C, 98% RH)	—	66
H_3BTC	MOF-808	3D	Solvothermal synthesis	7.58×10^{-3} (42 °C, 99% RH)	0.37	68
	MOF-808@PVDF-55	Film	Solution-casting method	1.56×10^{-4} (65 °C, hydrated in H$_2$O)	0.167	68
H_3BTC	MOF-808	3D	Solvothermal synthesis	8.97×10^{-6} (80 °C, 98% RH)	0.37	69
H_3BTC	MOF-808-EDTA	3D	Post-synthetic modification	1.31×10^{-4} (80 °C, 98% RH)	0.15	69
	MOF-808-ox	3D	Post-synthetic modification	4.25×10^{-5} (80 °C, 98% RH)	0.14	69
	MOF-808-ox@PVA-3	Film	Solution reaction	2.03×10^{-5} (80 °C, hydrated in H$_2$O)	—	69
H_3SNDC	VNU-17	3D	Solution reaction	6.65×10^{-6} (70 °C, 98% RH)	0.47	72
	Him9@VNU-17	3D	Post-treatment method	1.53×10^{-4} (70 °C, 98% RH)	0.44	72
	Him11@VNU-17	3D	Post-treatment method	5.93×10^{-3} (70 °C, 98% RH)	0.27	72
H_4TSNDC	VNU-23	3D	Solution reaction	1.54×10^{-4}(70 °C, 90% RH)	-	73
	His8.2@VNU-23	3D	Post-treatment method	1.79×10^{-2} (95 °C, 85% RH)	0.27	73

Table 1 (Contd.)

Organic linkages	MOFs	Structures	Syntheses	σ/S cm^{-1}	E_a/eV	Ref.
H$_2$TBNDC	Zr-BTNDC	3D	Solvothermal synthesis	7.88×10^{-5} (90 °C, 95% RH)	0.17	74
	Zr-BTNDC-ox	3D	Post-oxidation method	4.03×10^{-3} (95 °C, 95% RH)	0.22	74
	H@Zr-TBNDC-ox	3D	Post-acidification method	3.16×10^{-2} (90 °C, 95% RH)	0.25	74
H$_2$ox	((Me)$_2$NH$_2$)$_2$[Li$_2$(H$_2$O)$_4$Zr(ox)$_4$]	3D	Phase transition	3.9×10^{-5} (17 °C, 67% RH)	0.64	75
L-asp	MIP-202(Zr)	3D	Reflux with ambient pressure	0.011 (90 °C, 95% RH)	0.22	76
H$_2$fum	MOF-801	3D	Solvothermal synthesis	1.88×10^{-3} (25 °C, 98% R H)	0.256	77
	MOF-801@PP-60	Film	Solution-casting method	1.84×10^{-3} (52 °C, 98% R H)	—	77
H$_2$fum	C-SPAEKS/**Him-MOF-801-4**	Film	Solution-casting method	0.128 (90 °C, 100% RH)	—	78
	C-SPAEKS/**him@MOF-801-4**	Film	Solution-casting method	0.068 (90 °C, 100% RH)	—	78
3-H$_3$SPP	Zr(HPO$_4$)$_{0.65}$(3-HSPP)$_{1.35}$·nH$_2$O	2D	Solution reaction	0.04 (100 °C, 70% RH)	—	79
3-H$_3$SPP	10 wt%SPEESK(DS76%)/ZrSPP	Film	Solution-casting method	0.393 (120 °C, 100%RH)	—	80
	30 wt%SPEESK(DS34.6%)/ZrSPP	Film	Solution-casting method	0.23 (160 °C, 100%RH)	—	80
4-H$_3$SPP	Zr(HPO$_4$)$_{0.7}$(HO$_3$SC$_6$H$_4$PO$_3$)$_{1.3}$	2D	Solution reaction	0.063 (100 °C, 90% RH)	—	82
H$_8$CDTP	**1_lp@H**	3D	Post-treatment method	5.4×10^{-5} (80 °C, 95% RH)	—	83
	1_np@H	3D	Post-treatment method	6.6×10^{-5} (80 °C, 95% RH)	—	83
Glyphosate	G1	1D	Solution reaction	~10^{-3} (140 °C, 95% RH)	—	84
Glyphosine	G2	2D	Solution reaction	~10^{-3} (140 °C, 95% RH)	0.1	84
Glyphosine	G3	3D	Solution reaction	~10^{-4} (140 °C, 95% RH)	—	84
Glyphosine	ZPGly	2D	Solution reaction	1×10^{-3} (140 °C, 95% RH)	0.15	85
H$_6$FBTP	PCMOF20	2D	Phase transformation	1×10^{-2} (80 °C, 95% RH)	0.2	86
H$_6$TzGal	MIL-163	3D	Solvothermal synthesis	2.1×10^{-3} (90 °C, 95% RH)	0.25	90
THPP	ZrPP-1	3D	Solvothermal synthesis	8.0×10^{-3} (25 °C, 98% RH)	0.21	91
THBPP	ZrPP-2	3D	Solvothermal synthesis	4.2×10^{-3} (25 °C, 98% RH)	0.23	91

2. Proton conductive carboxylate Zr-MOFs

2.1. UiO-66 series MOFs

The three-dimensional porous MOF **UiO-66** is constituted of [Zr$_6$O$_4$(OH)$_4$] clusters with 1,4-benzenedicarboxylic acid (p-H$_2$BDC) linkages,[40] in which the pore structure is composed of a regular octahedral cage at about 11 Å and a regular tetrahedral cage at about 8 Å connected by a triangular window at about 6 Å. The dense structural units make the whole structure stable. At the same time, the Zr atom is highly oxyphilic, so the strong Zr–O bond also increases the stability of the structure. Therefore, **UiO-66** has high hydrothermal stability and chemical stability as well as mechanical stability. It can be stable at 500 °C, and can maintain its stable structure in water, DMF, benzene or acetone, and has strong acid stability and some alkalinity stability. These structural characteristics and outstanding structural stability are extremely beneficial for the research of proton conductivity.

2.1.1. Effect of defect control on proton conductivity. In 2015, H. Kitagawa and co-workers revealed the effect of defect control on the proton conductivity of UiO and its relevant MOFs.[44] Six MOFs, **Zr$_6$O$_4$(OH)$_{4.6}$(p-BDC)$_{5.7}$**, **Zr$_6$O$_4$(OH)$_{5.6}$(p-BDC)$_{5.2}$**, **Zr$_6$O$_4$(OH)$_{6.8}$(p-BDC)$_{4.6}$**, **Zr$_6$O$_4$(OH)$_4$(p-BDC)$_{5.3}$(OOCCH$_3$)$_{1.4}$**, **Zr$_6$O$_4$(OH)$_{4.8}$(p-BDC)$_{5.6}$** and **Zr$_6$O$_4$(OH)$_6$(p-BDC)$_5$** with different ligand defects were synthesized by changing the molar ratio of metal salt and ligand and adding different monocarboxylic acids (CH$_3$COOH and stearic acid). Since this topic was introduced in detail in our recent review,[33] it is briefly outlined here. They found that in addition to the number of ligand defects, the enhancement of the porosity of related MOFs and Lewis acid sites also can increase the σ value. The results indicate that at 65 °C and 95% relative humidity (RH), the proton conductivity (σ) of **Zr$_6$O$_4$(OH)$_6$(p-BDC)$_5$** can attain the highest value of 6.93×10^{-3} S cm^{-1} with the activation energy (E_a) being 0.22 eV. Although the proton conductivity of these MOFs prepared by ligand defect control is not very ideal, it provides us a new idea to regulate the proton conductivity by controlling the structural defects of UiO-based MOFs.

Based on the research of the influence of ligand defects on the σ value of **UiO-66**-based MOFs, the same group further explored the role of a 3D ordered defect sublattice on the acidity of a zirconium 2-sulfoterephthalate MOF.[45] The author first changed monosodium 2-sulfoterephthalic acid p-H$_2$BDC-SO$_3$H through ion exchange, and then reacted it with ZrCl$_4$ in H$_2$O to produce a MOF, **Zr$_6$O$_4$(OH)$_8$(p-BDC-SO$_3$H)$_{4.2}$·67H$_2$O**. Afterward, there is an ordered defect sublattice in the structure of the MOF by means of ICP-AES, CHN analysis, PXRD and ICP analysis and so on, and theoretical calculation. At the same time, they pointed out that the proton trapping nature of the defective sites of zirconium oxohydroxy clusters may cause the σ value of **Zr$_6$O$_4$(OH)$_8$(p-BDC-SO$_3$H)$_{4.2}$·67H$_2$O** to change little with RH and the value is ordinary. So they asserted that adding a certain amount of acids would saturate these proton capture sites and thus

3768 | *Inorg. Chem. Front.*, 2020, **7**, 3765–3784

This journal is © the Partner Organisations 2020

improve the proton conductivity of the resulting MOFs. Therefore, in the process of preparing $Zr_6O_4(OH)_8(p\text{-}BDC\text{-}SO_3H)_{4.2}\cdot67H_2O$, they added a certain amount of acetic acid and sulfoacetic acid respectively before reflux to synthesize MOFs, $Zr_6O_4(OH)_8(p\text{-}BDC\text{-}SO_3H)_4\cdot65H_2O$ and $Zr_6O_4(OH)_8(p\text{-}BDC\text{-}SO_3H)_4\cdot80H_2O$. And, they soaked $Zr_6O_4(OH)_8(p\text{-}BDC\text{-}SO_3H)_{4.2}\cdot67H_2O$ in 0.1 M H_2SO_4 aqueous solution for a day and got the MOF $Zr_6O_4(OH)_8(p\text{-}BDC\text{-}SO_3H)_{3.8}\cdot153H_2O$. PXRD determination verified that the four MOFs have similar structures. AC impedance analysis of them manifested that $Zr_6O_4(OH)_8(p\text{-}BDC\text{-}SO_3H)_4\cdot65H_2O$ treated with a weaker acid, CH_3COOH, had a σ value of 2.4×10^{-3} S cm^{-1}, which is slightly higher than that of pristine $Zr_6O_4(OH)_8(p\text{-}BDC\text{-}SO_3H)_{4.2}\cdot67H_2O$ $(1.93 \times 10^{-3}$ S cm$^{-1})$ at 65 °C and 95% RH. Interestingly, MOFs $Zr_6O_4(OH)_8(p\text{-}BDC\text{-}SO_3H)_4\cdot80H_2O$ and $Zr_6O_4(OH)_8(p\text{-}BDC\text{-}SO_3H)_{3.8}\cdot153H_2O$ treated with highly acidic $HO_3SCH_2CO_2H$ and H_2SO_4, respectively, have greatly enhanced σ values of 5.62×10^{-3} and 3.46×10^{-3} S cm^{-1}, respectively, at 65 °C and 95% RH. All the four MOFs displayed very similar E_a values around 0.25 eV implying that the proton transport obeys the hopping mechanism. Their research provides useful guidance for people to use defects in ZrMOFs and to regulate the proton conductivity through defect control.

2.1.2. Functionalized UiO-66-based MOFs. In the same year, J. R. Li *et al.* utilized the literature methods to prepare a series of **UiO-66**-based MOFs, **UiO-66-X** (X = SO$_3$H, 2COOH, NH$_2$, Br, H)[40,46–49] by modifying the p-H$_2$BDC ligand (Scheme 1), compared their proton conductivity and discussed the conductive mechanism.[50] The main structural features of these modified MOFs are the same as **UiO-66** MOF. Also, high thermal stability and high chemical tolerance were maintained. The proton conductivity of these compounds was determined by pressing pellet samples. They found that the σ value of the MOFs modified with –SO$_3$H and –COOH was greatly higher than that of MOFs modified with –NH$_2$ and –Br, as well as the original **UiO-66** MOF (Table 1). The maximum proton conductivity varies in the following order: **UiO-66-SO$_3$H** ≈ **UiO-66-(COOH)$_2$** > **UiO-66-NH$_2$** > **UiO-66** > **UiO-66-Br**. By means of the water vapor adsorption test, thermogravimetry-mass spectrometry and molecular simulation approaches, the influence of the substituted groups on the hydrophilicity and the formation of a H-bonded system was analyzed in detail. For example, molecular simulations evidenced that the H$_2$O affinity of these MOFs is following this order: **UiO-66-SO$_3$H** > **UiO-66-(COOH)$_2$** > **UiO-66-NH$_2$** > **UiO-66** > **UiO-66-Br**. The author believed that –SO$_3$H and –COOH groups are highly acidic, so they can be used as proton sources. Additionally, it is easy to compose a dense H-bonding system with adsorbed water molecules inside the framework, which is conducive to proton jumping. In general, they suggest that multiple factors, such as hydrophilicity, polarity, size, quantity, and acidity of substituents, influence the proton conductivity of functional MOFs.

Also in 2015, C. S. Hong and co-workers first used microwave-assisted solvothermal synthesis to form a sulfhydryl

(–SH) modified functional **UiO-66** MOF, **UiO-66-(SH)$_2$**, and then they used H$_2$O$_2$ post-oxidation to oxidize it to a sulfonic acid unit modified MOF, **UiO-66-(SO$_3$H)$_2$**.[51] Powder X-ray diffraction (PXRD) verified that both **UiO-66-(SO$_3$H)$_2$** and **UiO-66-(SH)$_2$** have the same phase as **UiO-66**. That is to say, the three compounds have basically the same structure. Like **UiO-66**, **UiO-66-(SO$_3$H)$_2$** and **UiO-66-(SH)$_2$** maintain their thermal stability at 400 °C and show excellent water stability by dipping in H$_2$O for thirty days and refluxing in H$_2$O. The N$_2$ adsorption test at −196 °C confirmed that the Brunauer–Emmett–Teller (BET) surface areas of these MOFs decreased with the increase of the substituent volume. For instance, BET areas are 897, 308 and 35 m^2 g^{-1} for **UiO-66**, **UiO-66-(SH)$_2$** and **UiO-66-(SO$_3$H)$_2$**, respectively. Consequently, they determined the σ values of these MOFs by using a pelletized sample from 25–80 °C under 90% RH. The maximum σ value of **UiO-66-(SO$_3$H)$_2$** is 8.4×10^{-2} S cm^{-1} at 80 °C and 90% RH, which is far greater than that of **UiO-66-(SH)$_2$** $(2.5 \times 10^{-5}$ S cm$^{-1})$ and of **UiO-66** $(4.3 \times 10^{-6}$ S cm$^{-1})$ under the same conditions. This can be interpreted by the hydroscopicity of the MOFs following the introduction of different substituents. **UiO-66-(SO$_3$H)$_2$** with acidic SO$_3$H units exhibits strong hydrophilicity, which will lead to the formation of hydrophilic channels in the framework for proton transport. In contrast, **UiO-66** and **UiO-66-(SH)$_2$** have lower water absorption ability. In addition, the high density of sulfonic acid groups in **UiO-66-(SO$_3$H)$_2$** is also one of the reasons for its super high proton conductivity. Note that the σ value of **UiO-66-(SO$_3$H)$_2$** at 25 °C and 90% RH $(1.4 \times 10^{-2}$ S cm$^{-1})$ is higher than that $(3.4 \times 10^{-3}$ S cm$^{-1})$ of **UiO-66-SO$_3$H** at 30 °C and ∼97% RH.[50]

In 2020, J. Banys *et al.* employed dielectric spectroscopy to investigate the water dynamics of two functionalized **UiO-66-NH$_2$** and **UiO-66-F$_4$** MOFs,[52] and discovered that both hydrated MOFs exhibit a tremendous dielectric dispersion, which can be divided into three overlapping processes. The three processes disappeared in the dehydrated sample, which suggests that the adsorbed H$_2$O units in the MOFs are the source of these three processes. This again indicates that although –NH$_2$ and –F groups have certain hydrophobicity, they can form H-bonds with the adsorbed H$_2$O units and thus enhance proton conductivity of the MOFs.

In 2019 S. K. Das *et al.*[53] reported two homologous MOFs, **PSM1** and **PSM2**, that were prepared by modifying **UiO-66-NH$_2$** through the sulfolactone reaction (Fig. 1). After **PSM 1**, **PSM 2** and **UiO-66-NH$_2$** were immersed in boiling water for seven
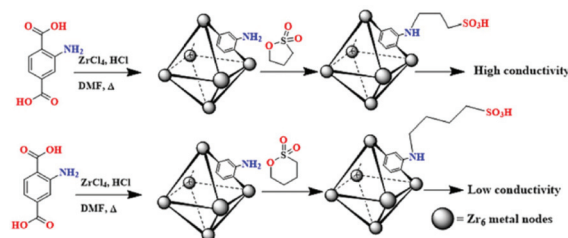

Fig. 1 The post-preparation routes of **PSM 1** (top) and **PSM 2** (bottom). Reproduced with permission from ref. 53. Copyright 2019, American Chemical Society.

This journal is © the Partner Organisations 2020

Inorg. Chem. Front., 2020, **7**, 3765–3784 | **3769**

days, respectively, they have similar PXRD patterns suggesting that they have similar structures and maintain their structural integrity even after treatment with boiling water. Moreover, both **PSM 1** and **PSM 2** had good thermal stability. As shown in Fig. 1, **PSM 1** and **PSM 2** have basically the same structure, except that the side chain length of the –SO$_3$H group is different, and the former is one less –CH$_2$ than the latter. Although it is only a small difference, the σ value of the two MOFs is fairly different. For example, at 80 °C and 95% RH, **PSM 1** has the highest σ value of 1.64×10^{-1} S cm^{-1}, while **PSM 2** only reaches 4.6×10^{-3} S cm^{-1} under the same conditions.

Apparently, different side chain lengths of –SO$_3$H groups may lead to different pK_a values. The pK_a value of the –SO$_3$H group in **PSM 1** (3.47) is smaller than that of the –SO$_3$H group in **PSM 2** (4.91), which may be the main reason why the σ value of **PSM 1** is greater than that of **PSM 2**. The lower pK_a constant causes the protons in the compound to dissociate more easily, resulting in higher proton conductivity. Because the spectral shifts of the N 1s XPS spectra of the two MOFs are the same, the influence of difference hydrogen bond networks inside the frameworks on the proton conductivity can be overlooked. They further analyzed theoretically the difference in the degree of dissociation of protons from sulfonic acid units in the two compounds, **PSM 1** and **PSM 2**, by the molecular electrostatic potential. The lower E_a values of **PSM 1** and **PSM 2** imply that proton transport within the two compounds follows a water-assisted hopping mechanism (also called the Grotthuss mechanism). Finally, it was found that the two compounds exhibited good stability and cycling usability after 48 hours of continuous AC impedance tests and five consecutive AC impedance tests with heating and cooling cycles.

In the same year, Y. Q. Lan and co-workers also used **UiO-66-NH$_2$** as the starting material to obtain two kinds of modified MOFs, **UiO-66-AS** and **IM-UO-66-AS** (Fig. 2), which kept the framework structure of **UiO-66-NH$_2$** and had good thermal and water stability.[54] As illustrated in Fig. 2, **UiO-66-AS** can be acquired by replacing part of 2-amino-terephthalic acid in **UiO-66-NH$_2$** with sodium 2-sulfoterephthalate, which has one more proton source and one more hopping site than **UiO-66-NH$_2$** (0 proton source, 1 hopping site). Furthermore, the uncoordinated amino group in **UiO-66-AS** was covalently connected with imidazole-2-carboxaldehyde through the Schiff base reaction to produce the MOF **IM-UiO-66-AS**, which had

one more proton source and two more hopping sites than **UiO-66-AS**. Obviously, **IM-UiO-66-AS** must exhibit an excellent σ value because it has the most proton sources and proton hopping sites (2 proton sources and 4 proton hopping sites). The results of AC impedance determinations also confirmed this conclusion. At 80 °C and 98% RH, the σ value of **IM-UiO-66-AS** is 1.54×10^{-1} S cm^{-1}, which is almost 3 and 5 orders of magnitude higher than **UiO-66-AS** (1.7×10^{-4} S cm^{-1}) and **UiO-66-NH$_2$** (3×10^{-6} S cm^{-1}), respectively, under the same conditions. Note that the σ value of **IM-UiO-66-AS** remained essentially unchanged after continuous testing at 80 °C and 98% RH up to 100 hours. In addition, the PXRD determinations also showed that the structure of the samples remained unchanged before and after the electrochemical test. These fully manifest the electrochemical stability of **IM-UiO-66-AS**, which offers a good foundation for future application.

The authors further doped the microcrystalline sample of **IM-UiO-66-AS** into a PVDF-PVP composite carrier to make a hybrid matrix film (called **IM-UiO-66-AS@PP**), and measured its proton conductivity and application in H$_2$/O$_2$ fuel cells. They discovered that the composite membrane revealed good stability, flexibility and σ value. When the weight of the doped MOF in the membrane is 60%, its σ value can be 1.19×10^{-2} S cm^{-1} at 80 °C and 98% RH. Nevertheless, the higher doping amount of the MOF did not bring the continuous improvement of the proton conductivity of **IM-UiO-66-AS@PP**. The composite film was applied to a H$_2$/O$_2$ fuel cell and its highest open circuit voltage (OCV) and power density were 0.78 V and 17.5 mW cm^{-2}, respectively (80 °C and 98% RH).

2.1.3 Experiment and molecular simulation to explore the proton conduction mechanism. The in-depth comprehension of the proton conducting mechanism is an important starting point for the research of proton conduction in crystalline solid materials. The complicated structure of Zr-MOFs is a challenge to the mechanism research. Therefore, people hope to deepen their understanding of the proton conduction mechanism by means of various experimental methods and theoretical calculations.

In 2014, the S. Devautour-Vinot group adopted broadband dielectric spectroscopy and molecular dynamics simulations to explore the water dynamics inside three Zr-MOFs, **UiO-66**, **UiO-66-COOH** and **UiO-66-(COOH)$_2$**.[55] Because the **UiO-66** framework is quite hydrophobic, there is a relatively weak interaction between water molecules and pore walls, which means that charge carriers are less likely to be generated in this solid, so **UiO-66** shows a low proton conductivity. However, molecular dynamics simulations indicated that the H$_2$O units can form clusters in the cages of **UiO-66**, which just absorbed very little water units. In contrast, **UiO-66-COOH** and **UiO-66-(COOH)$_2$** exhibit hydrophilicity due to the regulation of the polar –COOH groups. Accordingly, the σ value of **UiO-66-COOH** and **UiO-66-(COOH)$_2$** improves. The authors showed for the first time that the σ value of a MOF is related to water adsorption and the density of free carboxylic acids within the framework.
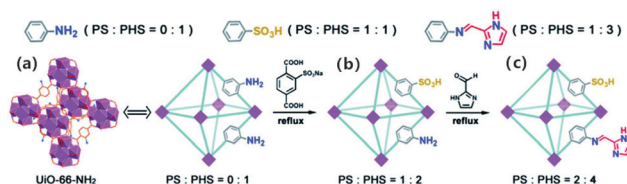

Fig. 2 Structure of **UiO-66-NH$_2$** (a); the preparation routes of post-modification **UiO-66-AS** (b) and **IM-UO-66-AS** (c) indicating the proton source (PS) and the proton hopping site (PHS). Reproduced with permission from ref. 54. Copyright 2019, Royal Society of Chemistry.

Later, the same group further studied the proton conduction mechanism of **UiO-66-(COOH)$_2$** at the molecular level by using the advanced quasi-elastic neutron scattering method (QNES) and aMS-EVB3 molecular dynamics simulations.[42] The QENS experiment shows that all protons are dynamically equivalent, and proton diffusion in the "clouds" around the oxygen atoms is caused by jumps between proton clouds. No diffusion of the O atom can be found. In addition, this research group also carried out aMS-EVB3 molecular dynamics simulation for **UiO-66-(COOH)$_2$** combining with QENS experiment, and verified that proton transport is mainly dominated by the Grotthuss mechanism, which is consistent with the calculated E_a value of 0.17 eV. Molecular dynamics simulations reveal that adsorbed water molecules within the framework can join the tetrahedron cages and neighbouring octahedral cages through hydrogen bonding bridges, namely by forming water hydrogen bonding networks between these cages, allow redundant proton hopping from a cage to another cage, to ensure that the excess protons can transfer for long distances, and thus ensure a higher σ value. For the first time, it has been expressed at the molecular level that long distance proton transport in a hydrated MOF is accomplished through a hydrogen-bonding network formed by water.

2.1.4 Composite membrane of UiO-66-based MOFs. As mentioned above, functional **UiO-66** series MOFs exhibit remarkable proton conductivity.[45,46,50,51,53,54,56] Nevertheless, their proton conduction pathways are not continuous enough, and it is intensely difficult to prepare a MOF membrane, which greatly limits their practical application. To overcome this problem, it is an effective method to introduce these functional Zr-MOFs into organic polymeric systems to prepare composite membranes.

In 2017, P. Y. Wu and co-workers doped separately or simultaneously two MOFs, **UiO-66-NH$_2$** and **UiO-66-SO$_3$H**, into Nafion and studied the σ value of the resulting composite films.[57] They found that the composite membrane containing both **UiO-66-NH$_2$** and **UiO-66-SO$_3$H** (denoted as **UiO-66-NH$_2$ + UiO-66-SO$_3$H/Nafion-0.6**) showed better performance than the single doped composite film (**UiO-66-SO$_3$H/Nafion-0.6** or **UiO-66-NH$_2$/Nafion-0.6**) in σ value, mechanical strength and methanol permeability. For example, at 90 °C and 95% RH, the proton conductivity of **UiO-66-NH$_2$ + UiO-66-SO$_3$H/Nafion-0.6** (0.6 presenting the weight percentage of the incorporated MOFs on the basis of Nafion) is 0.256 S cm^{-1} being about 1.17 times higher than that of the recast Nafion. The mechanism of these composite films was studied by water vapor adsorption and atomic force microscopy (AFM) and so on. The water vapor adsorption determination displayed that the co-doped composite film had the highest water absorption capacity under the synergistic action of the two hydrophilic functionalized Zr-MOFs. This indicates that denser hydrophilic channels can be formed in the composite membrane to facilitate proton transport. The AEM photos indicated that the interaction between the two MOFs, **UiO-66-NH$_2$** and **UiO-66-SO$_3$H**, with minor particle size and the ionic clusters in the membrane also resulted to the enhancement of the σ value. Meanwhile,

as both complexes have the ability to capture methanol molecules, the anti-methanol permeability of the composite film is greatly enhanced, which lays a foundation for the future application in DMFCs. Eventually, under extreme conditions (90 °C and 95% RH), the σ value of the membrane **UiO-66-NH$_2$ + UiO-66-SO$_3$H/Nafion-0.6** remained basically constant after continuous testing for 50 hours, showing superior durability.

Later, S. Q. Zang and co-workers again observed the synergistic effect of acidic and alkaline MOFs, **UiO-66-SO$_3$H** and **UiO-66-NH$_2$** with isomorphous structures on proton conductivity in the polymer chitosan (CS) in 2018.[58] Using the methods similar to those mentioned above, the proton conductivity of composite films for undoped and doped single MOF (**UiO-66-SO$_3$H** or **UiO-66-NH$_2$**) and doped two MOFs (**UiO-66-SO$_3$H** and **UiO-66-NH$_2$**) was compared. They discovered that the composite film bearing both **UiO-66-SO$_3$H** and **UiO-66-NH$_2$** manifested a remarkable σ value under hydrous (5.2×10^{-2} S cm^{-1} at 100 °C and 98% RH) and anhydrous conditions (3.78×10^{-3} S cm^{-1} at 120 °C) (Table 1). Note that the original σ value of **UiO-66-SO$_3$H** and **UiO-66-NH$_2$** at 100 °C and 98% RH was 3.4×10^{-3} and 1.4×10^{-5} S cm^{-1}, respectively, neither of which was extremely ideal. However, when they were mixed with CS and prepared into a composite membrane, **CS/UiO-66-SO$_3$H-6 + UiO-66-NH$_2$-15**, the effect of $1 + 1 > 2$ was produced, which indicated that both the MOFs and CS played an important role in the transmission of protons. As shown in Fig. 3, the SO$_3$H and NH$_2$ units from **UiO-66-SO$_3$H** and **UiO-66-NH$_2$** can interact with OH and NH$_3$ or NH$_2$ units of CS to establish abound H-bonded networks inside the composite film. Moreover, sulfonic acid groups can be used as proton sources in the absence or presence of H$_2$O, and NH$_2$ units can also be used as proton transport sites. In addition, NH$_2$ groups can form acid–base pairs with the sulfonic group of adjacent MOFs, which is very helpful for proton conductivity. The per-
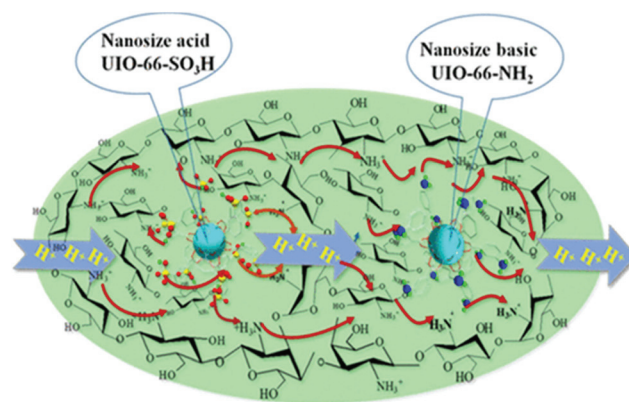

Fig. 3 Proposed schematic diagram of proton transport in the composite membrane, **CS/UiO-66-SO$_3$H-6 + UiO-66-NH$_2$-15**. Nanosize **UiO-66-SO$_3$H** and **UiO-66-NH$_2$** were simplified as a Zr$_6$O$_8$ cluster (solid blue ball) surrounded by 12 sulfonated benzoic acid and 12 amido benzoic acid, respectively. The pair of embedded MOFs in the CS matrix is interconnected with functional groups of CS-facilitated proton transfer. Reproduced with permission from ref. 58. Copyright 2018, American Chemical Society.

formance of the composite film in the H_2/O_2 fuel cell is that the OCV and power density are 1.0 V and 10.6 mW cm^{-2}, respectively.

In 2017, P. Y. Wu's group examined the σ value of **UiO-66-NH$_2$** combined with graphene oxide (GO) to get a composite membrane doped with Nafion.[59] The authors first chemically modified GO by coating the surface with polydopamine groups to facilitate the anchoring of **UiO-66-NH$_2$** by the Michael addition and Schiff base reactions. Subsequently, **GO@UiO-66-NH$_2$** dispersed in DMF solution was mixed with Nafion solution in DMF to obtain a **GO@UiO-66-NH$_2$/Nafion** composite film. Through the comparative study of these membranes, **GO/Nafion-0.6**, **UiO-66-NH$_2$/Nafion-0.6** and **GO + UiO-66-NH$_2$/Nafion-0.6**, the author observed that compared with the recast Nafion membranes, the σ value of these composite membranes is improved, but still cannot catch up with the proton conductivity of the **GO@UiO-66-NH$_2$/Nafion-0.6** film (σ: 0.303 S cm^{-1} at 90 °C and 95% RH) under the same test conditions. Moreover, **GO@UiO-66-NH$_2$/Nafion-0.6** can exhibit the highest anhydrous σ value of 3.403×10^{-3} S cm^{-1} at 120 °C. This indicates that the compound **GO@UiO-66-NH$_2$** obtained by the chemical reaction shows significant structural advantages after doping into the Nafion membrane. Obviously, homogeneous anchoring **UiO-66-NH$_2$** on the surface of GO is intensely beneficial to form a continuous proton transport channel. Moreover, the SO$_3$H units from Nafion and the –NH$_2$ units from **UiO-66-NH$_2$** can construct acid/base pairs providing the proton hopping sites. Additionally, **UiO-66-NH$_2$** has strong hydrophilicity. Thus, the above synergy leads to the composite film **GO@UiO-66-NH$_2$/Nafion-0.6** at high humidity or low humidity; even under anhydrous conditions it can efficiently transport protons. In addition, the authors also disclosed that when the doping amount of **GO@UiO-66-NH$_2$** is 0.6 wt%, the σ value of the composite membrane is the best; a lower or higher doping amount will lead to the performance degradation. The composite film **GO@UiO-66-NH$_2$/Nafion-0.6** also shows good methanol resistance and remarkable durability up to 54 hours.

Three year later, Y. Zheng and his colleagues made a covalent-ionically cross-linked **SPENs/UiO-66-NH$_2$** [SPENs = sulfonated poly(arylene ether nitrile)s] composite film and inspected its performance on the σ value, stability and MeOH permeability.[60] As expected, the composite membrane displayed wonderful thermal and dimensional stability due to the crosslinking effect and high stability of Zr-MOFs. Naturally, the NH$_2$ unit of **UiO-66-NH$_2$** is a good proton acceptor and donor, and thus the proton conductivity of the composite film can be greatly reinforced combining the interactions of NH$_2$ units with SO$_3$H and COOH of SPENs. For instance, the σ value of **SPEN/UiO-66-NH$_2$-5** can reach 1.351×10^{-1} S cm^{-1} at 80 °C in H$_2$O, which is higher than that of the recast SPEN. The MeOH permeability of the composite film can be suppressed because of the barrier effect of cross-linking and UiO-66-NH$_2$-x.

In 2020, W. Kang's group described that the MOF **UiO-66-NH$_2$** was firstly anchored with sulfonated poly(ether sulfone) (SPES) to prepare the **UiO-66-NH2@NF** nanofibers by the blend electrospinning approach.[61] And then, they found that inside the nanofibers, –SO$_3$H groups from SPES may form coherent proton transport channels with coordination of **UiO-66-NH**; in addition, the acid–base interaction between the –NH$_2$ units from **UiO-66-NH** and the –SO$_3$H units from SPES forms a channel-like ion cluster, which further promotes proton transport. These outstanding structural and performance advantages prompted the authors to further dope these nanofibers in the Nafion membrane to obtain a novel composite membrane with better performance. According to a series of determinations, such as SEM, TEM, PXRD, water adsorption, swelling ratio and AC impedance, the authors believed that the composite film **UiO-66-NH2@NFs-8/Nafion** with the loading amount of the MOF at 8% shows the best performance, and the σ value can reach 0.27 S cm^{-1} at 80 °C and 100% RH and excellent MeOH tolerability. The authors considered that the affinity between the nanofibers and Nafion membranes and the ability of the Zr-based MOF to capture methanol lead to the good resistance of the composite membrane to methanol permeability. Consequently, the composite film was applied to DMFC, and its OCV and the highest power density were 0.817 V and 95.49 mW cm^{-2}, respectively. These results indicate that the method of introducing Zr-MOFs to anchor nanofibers is worthy of further reference in the preparation of high-performance composite membranes in the future.

P. Y. Wu and co-workers first prepared the hybrid nanosheets **GO@UiO-66-SO$_3$H** by a simple method of *in situ* growth and thereafter doped it into the organic polymer poly (ether ether ketone) (SPEEK) to prepare the composite film in 2017.[62] As expected, the best σ value of the **SPEEK/UiO-66-SO$_3$H@GO-10** membrane can be 0.268 S cm^{-1} at 70 °C and 95% RH, which is 2.6 times higher than that of the recast SPEEK. Like the above doped Zr-MOF-based composite films,[43–45] the film **SPEEK/UiO-66-SO$_3$H@GO-10** shows strong mechanical properties and excellent methanol tolerance. As presented in Fig. 4, the authors proposed the feasible proton conduction mechanism.
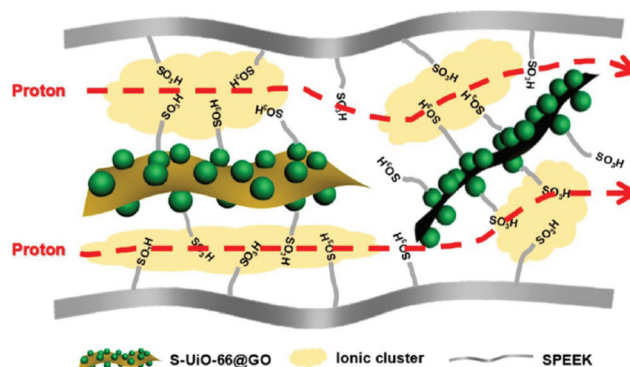

Fig. 4 Schematic diagram of the enhanced transport properties of **GO@UiO-66-SO$_3$H/SPEEK**. Reproduced with permission from ref. 62. Copyright 2017, American Chemical Society.

3772 | *Inorg. Chem. Front.*, 2020, **7**, 3765–3784

This journal is © the Partner Organisations 2020

First, the *in situ* growth method ensures uniform distribution of **UiO-66-SO₃H** on the GO surface, which provides a stable and continuous proton transport channel. Second, numerous sulfonic acid groups from SPEEK and **UiO-66-SO₃H** interact with each other to construct a denser and richer network of H-bonds with adsorbed H₂O units. Eventually, under the interaction of hydrophilic and hydrogen bonding between **UiO-66-SO₃H@GO** nanosheets and SPEEK, ion clusters and nanochannels are expanded and perfected, which is also very conducive to proton transport. To sum up, under the synergistic action of these functional units, the proton conduction efficiency of the composite membrane is greatly improved. Finally, MeOH crossover of the composite film was well reduced because of the barrier effect of **UiO-66-SO₃H@GO** nanosheets.

In 2017, the effects of the crystal size and filling amount of **UiO-66** and its sulfonated product **UiO-66-SO₃H** on the properties of the Nafion membrane were examined by F. Costantino *et al.*[63] For the **UiO-66/Nafion** film, they found that the composite film bearing a larger crystal (about 200 nm) in a low filling amount of 2% can attain the highest σ value of 0.207 S cm⁻¹ at 110 °C and 95% RH. The proton conductivity is reduced if the doped crystal is in small size (*e.g.* 20 nm) or if the filling amount is less than or greater than 2%. This conclusion is contrary to the conclusions of the previous papers,[43–48] which indicates the complexity of the research on proton conductivity in composite membranes. For the **UiO-66-SO₃H/Nafion** film, its σ value can reach 0.189 S cm⁻¹ at 110 °C and 95% RH when the filler loading is 2%, which is lower that of **UiO-66/Nafion-2** and slightly higher than that of pure Nafion (0.162 S cm⁻¹). This is also an anomaly, as the sulfonic acid functionalized zirconium complex **UiO-66-SO₃H** in the Nafion membrane should be more conducive to the formation of rich H-bonded networks. The authors believed that **UiO-66** acted as a modifier of the ionomer structural characteristics, which makes the proton conductivity enhance, and **UiO-66-SO₃H** may affect the σ value of the corresponding composite membrane in terms of its hydrophilicity and functional groups.

2.1.5 Composite membrane of *p*-H₂BDC-SO₃H-based heterometallic MOFs. For the convenience of description, a heterometallic MOF, **Zr-Cr-SO₃H**, constructed with the *p*-H₂BDC-SO₃Na ligand and its application in composite films are also described here. This MOF was solvothermally prepared by S. Neelakandan and co-workers in 2019.[64] For the purpose of comparative study, they also prepared an isostructural MOF, **UiO-66-SO₃H**, in accordance with a literature method.[40] Nitrogen adsorption and desorption experiments confirmed that the pore size and pore volume of the bimetallic compound were larger than those of **UiO-66-SO₃H**, which would facilitate rapid proton transmission and lead to the enhancement of proton conductivity for **Zr-Cr-SO₃H**. After that, they were used as fillers and mixed with a branched sulfonated polymer (BSP) to prepare composite membranes, respectively. All the prepared films indicated splendid stability in Fenton's solution. It is appropriate that the doping amount

of **Zr-Cr-SO₃H** is 0.5 wt%; the σ value of the relevant composite membrane **BSP/Zr-Cr-SO₃H-0.5%** is the highest (0.154 S cm⁻¹ at 80 °C and 100% RH) and higher than that of the **BSP/Zr-SO₃H-0.5%** film. When applied **BSP/Zr-Cr-SO₃H-0.5%** to DMFC, the OCV and maximum power density of the composite film are soared by 5% and 22%, respectively, compared with the pure BSP film, showing a good application prospect.
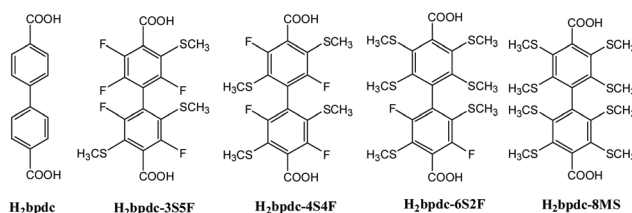
2.2. UiO-67 series MOFs

Because the MOF **UiO-67** has a similar crystal structure to **UiO-66**, except that it employs biphenyl-4,4′-dicarboxylic acid (H₂bpdc) replacing *p*-H₂BDC, like **UiO-66**, **UiO-67** has a mediocre proton conductivity. The reported proton conductive functionalized **UiO-67** MOFs are very limited. Scheme 2 gives organic linkages in the **UiO-67**-based MOFs.

In 2015, L. Liu's group synthesized the MOF **UiO-67** in accordance with the previously reported method,[48] and secondarily introduced imidazole (Him) units into the channels of this MOF by the evaporation method.[65] The imidazole molecules were filled in the micropores of the MOF and the framework structure of **Him@UiO-67** is similar to **UiO-67**. The results showed that the σ value of **UiO-67** was negligible in the measurement temperature range, and **Him@UiO-67** indicated a high σ value under anhydrous conditions, which may be because the introduction of imidazole increased the concentration of the proton carrier. Thus the σ value is positively related to the imidazole loading ratio and increasing temperature. The doped MOF **Him@UiO-67** attains a maximum σ value of 1.52×10^{-3} S cm⁻¹ at 130 °C under anhydrous conditions and a lower E_a value of 0.36 eV. Nevertheless, as the temperature is higher than 130 °C, the σ value began to decrease, which is possibly because the imidazole released from the micropores under high temperature conditions.

Obviously, the imidazole group in the framework not only provides the proton source, but also forms a hydrogen bond network with the framework component or constitutes a hydrogen bond network with each other to promote the proton hopping.

In 2020, J. He and co-workers obtained four boiling-water-stable modified **UiO-67**-based MOFs, **Zr-bpdc-3S5F**, **Zr-bpdc-4S4F**, **Zr-bpdc-6S2F** and **Zr-bpdc-8MS** through solvothermal synthesis with a systematic region-specific sulfur substituent (Scheme 2) and ZrCl₄ as starting materials.[66] Among them, a single crystal appropriate for X-ray diffraction for **Zr-bpdc-4S4F** is acquired. The framework of **Zr-bpdc-4S4F** is basically the

Scheme 2 The organic linkages appearing in the **UiO-67** series MOFs.

same as **UiO-67**, in which the secondary building unit (SBU) is a square-antiprismatic geometry formed by Zr^{4+} and the oxygen atoms in μ_3-O, μ_3-OH, –COOH units. Each SBU is connected to others through the ligand H_2bpdc-4S4F to form a ccp structure. The four MOFs exposed to air and dipped in boiling water were subjected to PXRD and gas adsorption measurements. The results depicted that they all showed excellent stability.

The researchers used 30% H_2O_2 to oxidize **Zr-bpdc-4S4F** to **Zr-bpdc-4SO$_2$Me4F**, in which four sulfide groups can be converted to sulfone functional groups confirmed by IR, ^{1}H and ^{19}F NMR determinations. Note that the framework of **Zr-bpdc-4S4F** was not damaged. The AC impedance of the two MOFs is measured. The results exhibit that the proton conductivity of **Zr-bpdc-4SO$_2$Me4F** is superior to its prototype. For example, **Zr-bpdc-4SO$_2$Me4F** has a σ value of 1.75×10^{-4} S cm^{-1} at 80 °C and 90% RH, which is about 1000 times higher than that of **Zr-bpdc-4S4F**. Apparently, a higher σ value of **Zr-bpdc-4SO$_2$Me4F** may be due to the increased hydrophilicity of these sulfone groups.

2.3. Other carboxylate-based Zr-MOFs

The proton conductivity of zirconium MOFs constructed from other carboxyl compounds (Scheme 3) is rarely studied, so it is summarized in this chapter.
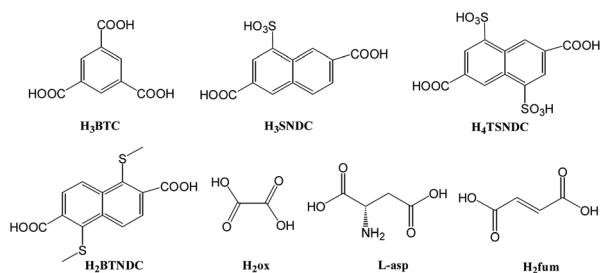
2.3.1. Trimesic acid-based MOFs. MOF-808 denotes a Zr-MOF of $Zr_6O_4(OH)_4(BTC)_2(HCO_2)_6$ (H_3BTC = trimesic acid), which was firstly solvothermally prepared by H. Furukawa and co-workers in 2014.[67] This MOF has similar Zr_6-oxoaggregates to that of **UiO-66**, and these clusters are connected by BTC^{3-} linkers to establish a three-dimensional framework with MTN topology and with two different hole cages (18.4 and 14 Å). Note that the HCOO$^-$ anions inside the framework could be replaced by OH$^-$ anions and water units by water washing or mild thermal treatment. So far, only one report on the proton conductivity of such complexes has been found.[54]

In 2017, X. M. Ren's group used H_3BTC to prepare **MOF-808**[68] in terms of the reported method.[67] The authors found that the compound remained structurally stable after immersion in ambient water or DMF for seven days, but decreased crystallinity after immersion in 80 °C hot water for four hours, indicating less stability in hot water. The proton conduction data of **MOF-808** at 99% RH and between 17 and

54 °C were tested by using a pressed sample tablet. The σ value of the MOF increases between 17 and 42 °C with the increase of temperature, and decreases above 42 °C. This phenomenon is obviously related to the structural instability of **MOF-808** accompanied by guest water molecules at high temperature. At 42 °C and 99% RH, the σ value is 7.58×10^{-3} S cm^{-1}. Interestingly, this compound displayed a high σ value at low temperatures. As an example, at 25 °C and 99% RH, its σ value can be 3.14×10^{-3} S cm^{-1}. Subsequently, the researchers further measured the effect of humidity on the proton conductivity of **MOF-808** at different humidity at 25 °C. The experimental data showed that the σ value has a serious dependence on humidity. Obviously, the adsorbed H_2O units in the lattice could establish a stable H-bonded network providing an effective way for proton transmission. Additionally, the E_a value of **MOF-808** is 0.37 eV showing that proton transport is mainly dominated by the Grotthuss mechanism.

Subsequently, this group fabricated a composite film **MOF-808@PVDF-x** (x denoting the mass percentage of **MOF-808**) by the casting method of mixing poly(vinylidene fluoride) (PVDF) and **MOF-808** in different mass percentages. PXRD and SEM analysis disclosed that the crystal structure of **MOF-808** remained well and was distributed evenly in the membrane. **MOF-808@PVDF-x** (x = 10, 25, 40, and 55) was immersed in deionized H_2O to measure its σ values. It was observed that the σ value of the composite membrane has certain temperature dependence, and also improved with the increase of the mass percentage of **MOF-808**. When the mass percentage was 55 wt%, the proton conductivity reached a maximum value of 1.56×10^{-4} S cm^{-1} at 65 °C. In addition, by comparing the σ value of the composite membrane with that of the pure PVDF membrane under the same conditions, it can also be discovered that the addition of **MOF-808** improves the σ value of the composite membrane. After immersion of **MOF-808@PVDF-55** in deionized H_2O for five days, it can still maintain high proton conductivity, indicating that the hybrid membrane has good durability. In addition, the E_a value of **MOF-808@PVDF-x** (x = 10, 25, 40, and 55) is less than 0.40 eV implying a Grotthuss mechanism.

Two years later, H. N. Wang and co-workers modified **MOF-808** with organic acids, ethylenediaminetetraacetic acid (EDTA) and H_2ox by the post-synthesis method and compared the proton conductivity of **MOF-808**, **MOF-808-EDTA** and **MOF-808-ox**.[69] What puzzled us was that the σ value of **MOF-808** they reported was much lower than that reported by Ren's group;[68] for example, the σ value of **MOF-808** reported by Wang's group is 1.25×10^{-6} S cm^{-1} at 30 °C and 98% RH, and the value reported by Ren's group is 3.14×10^{-3} S cm^{-1} at 25 °C and 98% RH. In addition, Wang's group believed that the σ value of **MOF-808** increased with the increase of temperature, but Ren *et al.* believed that the σ value decreased when the temperature was higher than 42 °C. We hypothesized that this may be due to different test methods or sample treatment methods, but the very different conductivity values remind us that the performance study of Zr-MOFs is complex and requires more care. Let's take a look at the results of compar-

Scheme 3 The organic linkages used in other carboxylate-based Zr-MOFs.

3774 | *Inorg. Chem. Front.*, 2020, **7**, 3765–3784

This journal is © the Partner Organisations 2020

ing the investigation of **MOF-808**, **MOF-808-EDTA** and **MOF-808-ox**.[55] by Wang's group. They found that after anchoring EDTA of H_2ox units, the proton conductivity can be augmented. For instance, at 80 °C and 98% RH, the proton conductivities of **MOF-808**, **MOF-808-EDTA** and **MOF-808-ox** are 0.897×10^{-5}, 1.31×10^{-4} and 4.25×10^{-4} S cm^{-1}, respectively. Additionally, the E_a values for the latter two modified MOFs are lower than that of **MOF-808**. Obviously, the two organic acids introduced into the framework can constitute hydrogen bond networks with adsorbed H_2O units to facilitate proton conduction; especially rigid oxalic acid can build up more efficient hydrogen bonded transport channels. In conclusion, the authors provide an effective method to optimize the proton conduction of the Zr-MOFs through post-synthesis, which is worthy of reference. They also studied the properties of the composite film, **MOF-808-ox@PVA-x**, and noticed that as $x = 3$, the σ value (2.03×10^{-5} S cm^{-1}) is the highest at 80 °C in water.

In 2016, H. A. Patel *et al.*[70] reported that the sulfonated **MOF-808** (**SZM**) that was synthesized by a literature approach,[71] was mixed with Nafion by the casting method. The composite film is denoted as **Naf-SZM**, in which the loading amount of **SZM** is assumed to be 1, 5, 7.5 and 10 wt%. From the SEM images of the composite films, it was found that when the SZM concentration exceeded 5 wt%, pinholes and cracks appeared in the film, and the compatibility of **SZM** and Nafion would also decrease. Finally, it was found that 1 wt% was the optimal concentration of **SZM**, and the composite film under this condition also had good stability at 300 °C. When the humidity is 35% RH, the composite membrane shows better proton conductivity and higher performance stability than Nafion. They believed that **SZM**'s superacidity sites improve the water uptake in the film and thus are helpful for long-distance proton conduction. By monitoring the OCV 24 hours, they discovered that the composite film **Naf-1SZM** showed high performance stability at low humidity (35% RH) and 80 °C in fuel cells. This experimental result once again proves that the acidic sites introduced by post-treatment can boost the σ value of the Zr-MOFs and the performance of the corresponding composite membranes, which is very beneficial for practical application in the future.

2.3.2. Naphthyl acid-based Zr-MOF. In 2017, T. N. Tu and co-workers adopted a naphthyl-based organic ligand bearing several Brønsted acid sites, 4-sulfonaphthalene-2,6-dicarboxylic acid (H_3SNDC), to react with $ZrOCl_2 \cdot 8H_2O$ in DMF solution in the presence of HCOOH producing a new 3D MOF, $[Zr_6O_8(H_2O)_8(HSNDC)_4] \cdot 15H_2O$ (denoted as **VNU-17**, VNU = Vietnam National University).[72] As indicated in Fig. 5, **VNU-17** presents the bcu topology and is composed of $Zr_6O_8(H_2O)_8(COO)_8$ clusters bridged by 2-connected SNDC^{3-} ligands resulting in a three-dimensional porous framework with 6 Å pore channels. Consequently, they employed a simple method to immerse **VNU-17** in different concentrations of imidazole (1 M or 5 M) in MeOH solutions for one day or two days. Thus, two MOFs, **Him5@VNU-17** and **Him11@VNU-17**, with different imidazole loadings were acquired. PXRD deter-
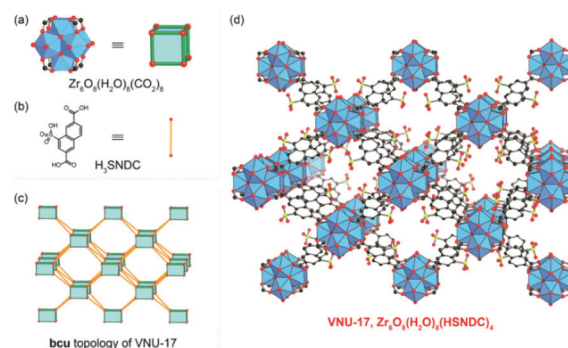

Fig. 5 The crystal structure of **VNU-17** is built by eight-connected, cubic $Zr_6O_8(H_2O)_8(COO)_8$ clusters (a) joined by linear, ditopic HSNDC^{2-} linkers (b) to construct a structure showing the bcu topology (c, view from the [001] plane). The framework of **VNU-17**, $Zr_6O_8(H_2O)_8(HSNDC)_4$, is depicted (d). Atom colors: Zr, blue polyhedra; C, black; O, red; S, yellow. All H atoms are omitted for clarity. Reproduced with permission from ref. 72. Copyright 2017, the Partner Organisations.

minations indicated that the structures of the three MOFs are the same. The results of thermal analysis revealed that the loss of imidazole groups in both complexes **Him5@VNU-17** and **Him11@VNU-17** occurred at more than 200 °C, which lays a material foundation for conducting proton research.

Furthermore, ac impedance spectroscopy measurements indicated that at a fixed temperature of 70 °C, the σ values of the three MOFs are humidity dependent, and increase with the increasing RH. Among them, the σ value of **Him11@VNU-17** is the largest, which attains a maximum value of 5.93×10^{-3} S cm^{-1} under 98% RH, and the smallest is **VNU-17**. Note that over all RH ranges, **Him11@VNU-17** with higher loading always has a higher σ value than **Him9@VNU-17** with lower loading. Another thing to note is that the proton conductivity of **Him11@VNU-17** is 900 times higher than that of the parent complex **VNU-17** under 70 °C and 98% RH. Although sulfonic acid groups provide protons more easily than imidazolium ions, the high polarity of imidazolium ions completely hydrates the entire pores and grain boundaries and promotes the formation of a proton conductive network, so the proton conductivity of anchored MOFs is greater than that of unanchored MOFs. Note that the σ value of **Him11@VNU-17** can be maintained for at least 40 hours and the structure does not change, which proves that its stability and durability of proton conductivity are excellent. In addition, the calculated E_a values of **Him11@VNU-17**, **Him9@VNU-17** and **VNU-17** are 0.27, 0.44 and 0.47 eV, respectively. This shows once again that **Him11@VNU-17** with a high loading of Him is more likely to form a dense hydrogen bond network, which is conducive to proton hopping.

Later, the same group prepared a similar MOF $[Zr_6O_8(H_2O)_8(H_2TSNDC)_4]$ namely **VNU-23** by using 4,8-disulfonaphthalene-2,6-dicarboxylic acid (H_4TSNDC) and $ZrOCl_2 \cdot 8H_2O$,[73] whose structure is similar to **VNU-17**, and the $Zr_6O_8(H_2O)_8(COO)_8$ cluster is connected by TSNDC^{4-} linkages. By using a simple method similar to that described above,

VNU-23 was immersed in 0.5 M histamine (His) methanol solution for three days. Subsequently, His was anchored on **VNU-23** to obtain **His8.2@VNU-23** confirmed by ^{1}H NMR, EA and single crystal X-ray diffraction. The protonated histamine can interact with SO_3H units as well as coordinate with H_2O units to constitute extended hydrogen bond networks. The σ value of **His8.2@VNU-23** is greater than that of **VNU-23**, and the maximum value is 1.79×10^{-2} S cm^{-1} at 90 °C and 85% RH. When exploring the effect of temperature on the proton conductivity of **His8.2@VNU-23**, it was found that the σ value did not continue to decrease at 90–30 °C, but there was a step-wise increase at 60–50 °C. This situation may be related to the protonated histamine rearrangement. **His8.2@VNU-23** has a lower E_a value of 0.27 eV suggesting that the Grotthuss mechanism can be observed.

In 2020, by adopting 1,5-bis(methylthio)naphthalene-2,6-dicarboxylic acid (H_2BTNDC) and $ZrCl_4$, J. He and co-workers solvothermally synthesized a porous MOF $\{[Zr_6O_8(H_2O)_8(BTNDC)_4]\cdot 9DMF\}_n$, namely **Zr-BTNDC**,[74] in which 8-connected $Zr_6O_8(H_2O)_8(COO)_8$ clusters were connected by BTNDC^{2-} ligands forming a three-dimensional network with 6 Å pore channels. The oxidized product **Zr-BTNDC-ox** was obtained by stirring **Zr-BTNDC** in a solution of 30% H_2O_2 aqueous solution for one day. ^{1}H NMR spectra confirmed that SCH_3 units were oxidized to sulfoxide or sulfone units. The PXRD pattern of the oxidized product is almost the same as that of **Zr-BTNDC**, indicating that the structure has not changed. Consequently, **Zr-BTNDC-ox** was put into 0.05 M sulfuric acid solution for seven hours to get the acidic framework, **H@Zr-BTNDC-ox**. The PXRD test indicates that the structure of the acidized product has not changed but the crystallinity has decreased. Further electrochemical measurements showed that the post-treatment method (oxidation and acidification) enhanced the σ value of the resulting MOFs. It should be noted that the proton conductivity of the three complexes improves with the rise of temperature or humidity. Under similar conditions, the σ value of **H@Zr-BTNDC-ox** is 3.16×10^{-2} S cm^{-1} (90 °C and 95% RH), which is almost 10 times higher than that of **Zr-BTNDC-ox** (4.03×10^{-3} S cm^{-1} at 95 °C and 95% RH), and is 400 times higher than that of **Zr-BTNDC** (7.88×10^{-5} S cm^{-1} at 90 °C and 95% RH). At the same time, the E_a values of the three complexes are lower than 0.4 eV at both 85% and 95% RH, indicating that proton conduction in the frameworks follows the Grotthuss mechanism. From the structural analysis, it is easy to understand this phenomenon. In the acidification and oxidation of MOFs, H_2O units, sulfones, sulfoxide and sulfate groups can all act as proton carriers and interact to form more complex hydrogen bond networks, which are more conducive to proton transport. In pristine **Zr-BTNDC**, only coordinated H_2O and absorbed H_2O units can take part in the proton transport.

2.3.3. Oxalic acid-based Zr-MOF. In 2015, S. Tominaka and co-workers[75] described a rare phenomenon of a 3D MOF $((Me)_2NH_2)_2[Li_2Zr(ox)_4]$ (H_2ox = oxalic acid) containing lithium and zirconium metals under humidity stimulation from insulator to proton conductor, and analyzed the reasons for this phenomenon through single crystal X-ray diffraction and X-ray pair distribution function analysis. Under the stimulation of humidity, this compound presents three phase transitions: when humidity is less than 50% RH, it is the phase I state, and its formula is $(Me_2NH_2)_2[Li_2Zr(ox)_4]$, in which there is no coordination water, so it is a non-conductor. When the RH is raised to 67%, the structure is transformed into phase III, in which there are four coordination water molecules, which can act as a proton source and rapidly increase the σ value of the compound to 3.9×10^{-5} S cm^{-1} at 17 °C. When the RH is reduced to 25% again, the compound is converted to phase II, and its chemical formula is $(Me_2NH_2)_2[Li_2(H_2O)_{0.5}Zr(ox)_4]$ tested by single crystal X-ray diffraction, despite the presence of a coordination water molecule, because the water can H-bond with ox^{2-} anions, and the compound cannot conduct protons. When the humidity is raised to 67% RH, the compound conducts protons again. Therefore, this MOF can be used as a humidity dependent conductivity-switching device.

2.3.4. Amino acid-based Zr-MOF. A three-dimensional Zr-MOF **MIP-202 (Zr)** self-assembled by a natural amino acid, L-aspartic acid (L-asp), and $ZrCl_4$ was reported in 2018.[76] The preparation of this compound is very convenient and green and can be produced in large quantities. What's more, the structure of this compound is very stable; for example, it can be stable in aqueous solution with a pH range of 0–12 and boiling water. Its crystal structure is isostructural to the earlier prepared cubic (fcu topology) Zr-fumarate MOF namely **MOF-801**.[52] In this MOF, the $Zr_6(\mu_3\text{-}O)_4(\mu_3\text{-}OH)_4$ clusters were connected by L-aspartate linkages to construct a three-dimensional framework, in which NH_2 units are all protonated and coexist with chloride anions to constitute NH_3^+/Cl^- pairs. Therefore, ammonium cations in the cavity of the framework can be used as a proton source and form a hydrogen bond network with the absorbed water molecules to facilitate proton transport. In addition, a large number of highly electronegative and hydrophilic chlorine ions in the cavity can also build up a great number of hydrogen bonds with water molecules to facilitate proton transport. Naturally, a super high σ value of 0.011 S cm^{-1} at 90 °C and 95% RH can be observed. A lower value of activation energy (0.22 eV) also predicts that the proton transfer is in accord with the hopping mechanism, which is also consistent with the above structural analysis.

2.3.5. Unsaturated fatty acid-based Zr-MOF. In 2018, by employing $ZrOCl_2\cdot 8H_2O$ and fumaric acid (H_2fum), X. M. Ren's group prepared a three-dimensional MOF **MOF-801** in the light of a literature method,[66] and explored its stability, proton conductivity and application in composite films and fuel cells.[77] The crystal structure of the compound is simply described as follows: each Zr-oxide SBU containing six Zr^{4+} atoms bridged by eight μ_3-O atoms (four OH units and four O^{2-} anions) are joined by linear and ditopic fumarate bridges to constitute a three-dimensional framework having porous tetrahedral and octahedral cages. Ren *et al.* further confirmed that the MOF has remarkable acidic (6 M) and diluting basic (0.1 M) stability. The variable-temperature PXRD test showed that it can hold its structure up to 250 °C. Further

3776 | *Inorg. Chem. Front.*, 2020, **7**, 3765–3784

This journal is © the Partner Organisations 2020

electrochemical experiments ascertained that the proton conductivity of the MOF was temperature and humidity dependent. At 61 °C and 98% RH, its σ value can be 4.16×10^{-3} S cm^{-1} with a lower E_a of 0.256 eV obeying the Grotthuss mechanism. At the same time, time-dependent impedance determination demonstrated that its proton conductivity is basically constant under 25 °C and 98% RH for eight days. Subsequently, the MOF was doped in poly(vinylidene fluoride)-poly(vinylpyrrolidone) as a filler, and it was found that the σ value of the composite membrane **MOF-801@PP-X** increased with the increase of the doping amount of **MOF-801**. **MOF-801@PP-60** showed the highest σ value of 1.84×10^{-3} S cm^{-1} at 52 °C and 98% RH. Finally, the composite film was utilized in a H$_2$/O$_2$ fuel cell, resulting in an OCV of 0.95 V at 30 °C and 100% RH.

In 2020, considering that the pore size (7.4 Å) of **MOF-801** is suitable for the introduction of imidazole units (4.3×3.7 Å^2), Z. Zhang and co-workers introduced imidazole into this framework in two different ways (impregnation and *in situ* methods) to prepare two related MOFs, **Him@MOF-801** with free imidazole units incorporating inside the pores and **Him-MOF-801** with imidazole coordinating with the zirconium atoms.[78] PXRD determinations demonstrated that the structures of the three compounds are basically the same, although the imidazole introduced has a slight effect on the strength and position of some diffraction peaks. Moreover, after soaking in 80 °C H$_2$O and 1 M hydrochloric acid aqueous solution for seven days, the two compounds **Him@MOF-801** and **Him-MOF-801** remained structurally rigid. This lays a material foundation for their application in membrane systems.

Subsequently, this group employed the solution casting approach to make hybrid membranes with **Him@MOF-801** or **Him-MOF-801** as fillers and sulfonated poly(arylene ether ketone sulfone) containing carboxyl groups (C-SPAEKS) as the organic matrix. The composite membrane can be expressed as **C-SPAEKS/Him@MOF-801-X** and **C-SPAEKS/Him-MOF-801-X** (*X* presents the mass percentage of MOFs). Since the doped MOFs are combined with C-SPAEKS through hydrogen bonding, the stability of the hybrid membrane is higher than that of the pure C-SPAEKS film. Meanwhile, the addition of MOFs increases the water absorption of the hybrid membrane and has a positive correlation with the mass percentage of MOFs. On this basis, the σ value of the hybrid membrane was explored. At 100% RH and 30–90 °C, the σ value of the hybrid membrane increases with increasing temperature. Comparing with the σ value of pure C-SPAEKS under the same testing conditions, the addition of MOFs improved the proton conductivity of the hybrid membrane, and 4% is the optimal filling amount of MOFs. At 100% RH and 90 °C, **C-SPAEKS/Him-MOF-801-4** reached the maximum σ value of 0.128 S cm^{-1}, which was twice that of **C-SPAEKS/Him@MOF-801-4**. In general, the two composite films exhibited high proton conductivity. This manifests that both the free imidazole groups in the pores and the coordination imidazole groups in the frameworks play a key role in improving the proton conductivity. The difference in proton conductivity between the two

composite membranes is that the imidazole involved in coordination is more likely to provide protons than coordination H$_2$O units. A **C-SPAEKS/Him-MOF-801-4** film was used in DMFC to determine its performance. The OCV at 80 °C was 0.75 V, and the maximum power reached 15.4 mW cm^{-2}.
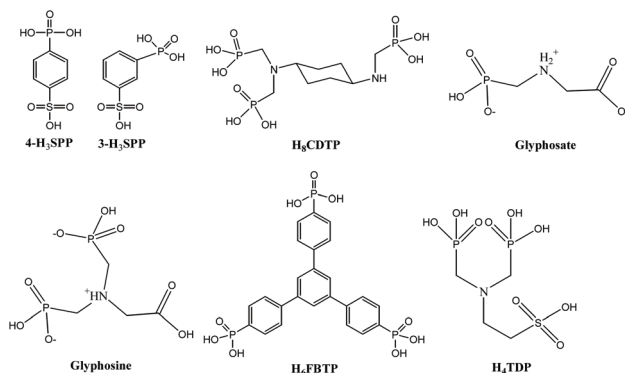
In one word, through the introduction of imidazole units into Zr-MOFs (**UiO-67**,[65] **VNU-17**[72] or **MOF-801**[76]), we can find that both free imidazole groups in the pores and imidazole units involved in the coordination of zirconium ions, all the resulting MOFs indicate a greatly improved proton conductivity under hydrous or anhydrous conditions. It can be seen that this is an efficient strategy to strengthen the proton conductivity of zirconium-based MOFs.

2.4. Phosphate-based MOFs

The organic ligands containing phosphate groups usually exhibit a strong coordination ability and various coordination modes by protonated species, so a large number of phosphate-based MOFs can be constructed. L. M. Zheng's group has reviewed the proton conductive phosphate-based MOFs.[32] Nevertheless, the research of proton conduction in zirconium-based phosphate MOFs is very limited. Scheme 4 presents phosphate ligands used in proton conducting Zr-MOFs.

In 2005, G. Alberti and his colleagues prepared a series of Zr-MOFs with the general formula Zr(HPO$_4$)$_{2-x}$(3-HSPP)$_x$·nH$_2$O (3-HSPP = 3-sulfophenyl phosphoric acid; x in the range 0.4–1.35).[79] From the PXRD patterns of these MOFs, they speculated that these compounds were layered structures. Proton conductivity investigations indicated that as $x = 1.35$, the MOF had a maximum σ value of 0.04 S cm^{-1} at 100 °C and 70% RH. Obviously, phosphate groups present are responsible for the high σ value of the MOF **Zr(HPO$_4$)$_{0.65}$(3-HSPP)$_{1.35}$·nH$_2$O**.

Five years later, Z. Li and co-workers prepared SPPESK/ZrSPP composite membranes composed of sulfonated poly(phthalate ether sulfone ketone) (SPPESK) and the MOF **ZrSPP** bearing 3-H$_3$SPP ligands by solution casting.[80] **ZrSPP** exhibits a layered structure,[81] is insoluble in H$_2$O, has good thermal stability, and is an excellent alcohol barrier. **ZrSPP** can dis-

Scheme 4 The organic linkages used in phosphate-based Zr-MOFs.

This journal is © the Partner Organisations 2020

Inorg. Chem. Front., 2020, **7**, 3765–3784 | **3777**

perse uniformly in **SPPESK**, and strong H-bonds can be formed between them. The TGA curve indicated that the composite membrane has high enough stability to be used in DMFCs. The AC impedance experiment was performed on composite membranes with different **ZrSPP** loadings. As the temperature increased, the σ value of the composite membranes increased significantly (>80 °C). Compared with the pure SPPESK membrane, the σ value of the composite membrane is higher, and the σ value of the composite membrane decreases with the increase of the **ZrSPP** loading. When temperature was lower than 80 °C, the proton conductivity of **SPPESK(DS34.6%)/ZrSPP** (DS means degrees of sulfonation of SPPESK) is lower than that of **SPPESK(DS76%)/ZrSPP**, indicating that SPPESK plays a major role in proton conduction at low temperature, and a higher DS will have more sulfonic acid units support proton transfer. As the temperature continued to rise, it was found that the maximum value appeared at 120 °C, which may be due to the hydrophilicity of SO_3H, and the composite membrane with a high DS was easy to expand, so its structure could not be maintained for a long time at high temperature. In addition, the researchers found that with the addition of **ZrSPP**, the elasticity of the composite membrane will become weaker, but at the same time it will also increase the oxidation resistance of the composite membrane. In general, a low DS of SPPESK and a high concentration of ZrSPP are beneficial to improve the thermal stability of the composite membrane. The hybrid membrane prepared by this group not only has a good σ value and low MeOH permeability, but also can increase the thermal stability of the membrane by adjusting the amount of raw materials, laying a foundation for future practical applications.

In 2010, V. Zima's group[82] successfully synthesized two proton conductive layered MOFs, $Zr(HO_3SC_6H_4PO_3)_2·2H_2O$ and $Zr(HPO_4)_{0.7}(HO_3SC_6H_4PO_3)_{1.3}·2H_2O$ under hydrothermal conditions by using a similar ligand 4-sulfophenyl phosphoric acid (4-H_3SPP) and $ZrOCl_2·8H_2O$. Adopting PXRD patterns, they also speculated that the two compounds were layered structures, in which an interlayer distance of about 19.9 Å can be calculated, and the Zr^{4+} and six oxygen atoms of the phosphonate group form an octahedral geometry. The σ value of the two MOFs is sensitive to humidity and temperature variations. That is, their proton conductivity rises with temperature or humidity. It's important to note that the σ value of $Zr(HPO_4)_{0.7}(HO_3SC_6H_4PO_3)_{1.3}·2H_2O$ is much higher than that of $Zr(HO_3SC_6H_4PO_3)_2·2H_2O$ under the same test conditions. They suggested that the presence of phosphate groups in $Zr(HPO_4)_{0.7}(HO_3SC_6H_4PO_3)_{1.3}·2H_2O$ leads to structural disorder that increases the number of "labile" protons and changes their behavior compared to $Zr(HO_3SC_6H_4PO_3)_2·2H_2O$, and that $Zr(HPO_4)_{0.7}(HO_3SC_6H_4PO_3)_{1.3}·2H_2O$ can absorb more water molecules than $Zr(HO_3SC_6H_4PO_3)_2·2H_2O$, which results in an increase in the σ value. Nevertheless, both the two MOFs not only show high proton conductivities, but also are insoluble in H_2O and have high thermal stability. They are all expected to become a component of the proton exchange membrane of the fuel cell.

In 2012, F. Costantino and co-workers reported two open framework Zr-MOFs, $Zr(H_4CDTP)_2Na_2H_2·5H_2O$ or $Zr(H_4CDTP)_2(NH_4)_2H_2·5H_2O$ (denoted as **1_lp@Na** and **1_lp@NH₄**, respectively; lp means large pore) (H_8CDTP = cyclohexyl-*N,N,N′,N′*-diamino tetraphosphoric acid, Scheme 4) under solvothermal conditions.[83] The flexible MOF has rectangular channels of size 12 × 5 Å, which are occupied by five H_2O units and two Na^+ or NH_4^+ cations per formula unit, and with eight PO_3C tetrahedra pointing to the inner space. The fully protonated phase **1_lp@H** could be acquired by putting **1_lp@Na** and **1_lp@NH₄** into 0.2 M HCl aqueous solution. Then the authors found that there was a phase transition process: when **1_lp@H** is heated above 150 °C, an anhydrous phase (hereafter **1_an**) can be obtained. However, when **1_lp@Na** or **1_lp@NH₄** was heated, **1_an** could not be obtained. This is because the cations in **1_lp@Na** or **1_lp@NH₄** can retain H_2O and template the framework. Interestingly, after dipping **1_an** into H_2O for a few minutes or putting aside in air for 3–4 days, a new phase **1_np@H** (np means narrow pore) can be produced. After heating **1_np@H** up to 150 °C, phase **1_an** can be recovered. They adopted PXRD determinations and Rietveld refinements to explain the transformation mechanisms. As indicated in Fig. 6, in the
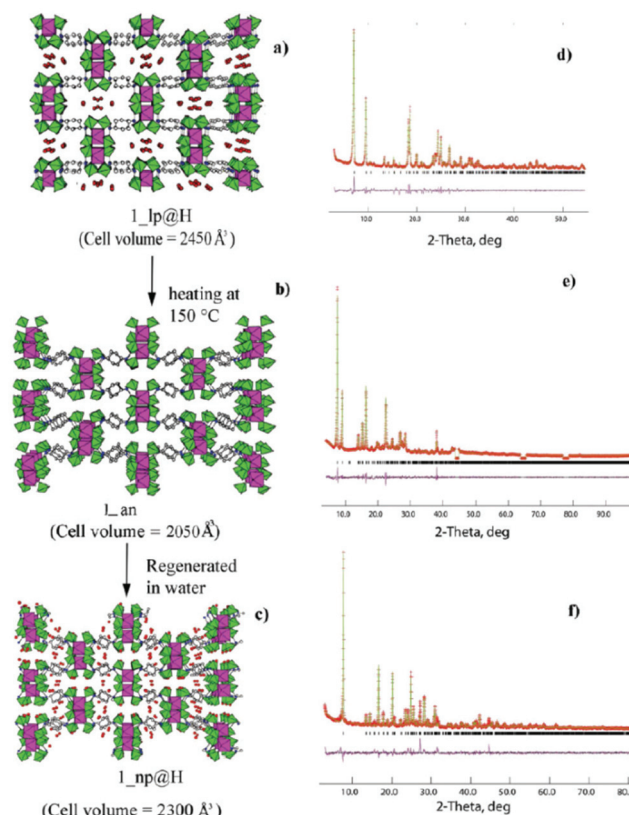

Fig. 6 Structure representation and the corresponding Rietveld plots for **1_lp@H** (a), **1_an** (b), and **1_np@H** (c). Note that **1_lp@H** and **1_np@H** are full crystallographic structures whereas **1_an** is only a possible structural model based on the cell parameters. Reproduced with permission from ref. 83. Copyright 2012, American Chemical Society.

compounds **1_lp@H** and **1_np@H**, the position of crystallization H_2O units in the cavity and the hydrogen bond formed changed obviously.

Consequently, they further explored the proton conductivity of **1_lp@H** and **1_np@H**, and found that at 95% RH, the σ value of **1_lp@H** changed from 2.6×10^{-5} (30 °C) to 5.4×10^{-5} S cm^{-1} (80 °C), and the value of **1_np@H** varied from 1.5×10^{-6} (30 °C) to 6.6×10^{-6} (80 °C) S cm^{-1}. They believed that there is a strong hydrogen bond system in **1_lp@H** and the stretching along two directions is conducive to the hopping of protons, while the hydrogen bond in **1_np@H** is weak and has only one direction, resulting in a weaker conductivity of **1_np@H** than **1_lp@H**.
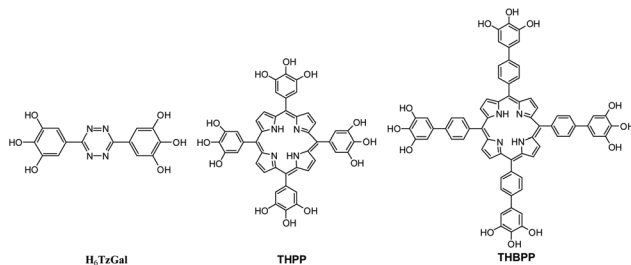
In 2013, three MOFs, **ZrF[H$_3$(O$_3$PCH$_2$NHCH$_2$COO)$_2$]** (**G1**), **Zr$_3$H$_8$[(O$_3$PCH$_2$)$_2$NCH$_2$COO]$_4$·2H$_2$O** (**G2**), and **Zr[(O$_3$PCH$_2$)(HO$_3$PCH$_2$)NHCH$_2$COOH]$_2$·2H$_2$O** (**G3**) with different structures were prepared by using two phosphono-amino acid ligands (glyphosine and glyphosate).[84] The crystal structures of **G1** and **G2** were obtained from *ab initio* PXRD data. The crystal structure of **G3** was obtained by single crystal X-ray diffraction. Structural analyses display that **G1** is a 1D ribbon-like framework, while **G2** shows a layered structure and **G3** indicates a 3D framework. The trend of the proton conductivity of the three MOFs with temperature change was measured at 95% RH. It was found that the σ value of **G2** increased slightly with temperature rise, while that of **G1** and **G3** increased significantly, increasing by 4 and 10 times, respectively. The σ value of **G3** is at least an order of magnitude lower than that of **G1** and **G2**. The authors believed that the large surface area of **G1** and **G2** in comparison with **G3** may lead to their higher σ values. During the measurement, it was found that the proton conductivity and hydration of **G2** had a weak dependence on temperature. Using the Arrhenius equation, the calculated E_a value of **G2** was 0.10 eV, and the conduction mechanism was the Grotthuss mechanism. Note that the highest σ value of **G1** and **G2** reaches up to 10^{-3} S cm^{-1} at 140 °C and 95% RH. As they have a good σ value, and high thermal stability, they are expected to be good proton conductive materials.

In 2014, the same group still used glyphosine as a starting material to synthesize a new MOF under mild reaction conditions, whose molecular formula is **Zr$_2$(PO$_4$)H$_5$((O$_3$PCH$_2$)$_2$NCH$_2$COO)$_2$·H$_2$O** (**ZPGly**).[85] Its structure was also obtained by the calculation method as previously reported.[82] The layered structure of **ZPGly** is composed of a ZrO$_6$ octahedron built by tetradentate PO$_4$ groups and Zr^{4+} atoms. The uncoordinated –COOH and P–OH units are exposed to the sheet surface. Obviously, the large number of these hydrophilic groups between layers will contribute greatly to proton conduction. As expected, the σ value of this MOF is highly dependent on RH and can attain the highest value of 1×10^{-3} S cm^{-1} at 140 °C and 95% RH. In addition, the researchers investigated the hydration of this MOF in different humidity ranges and found that the overall hydration of **ZPGly** has little effect on the σ value, and the change in conductivity only reflects the change in the hydration of the crystal surface. It can be said that the σ value is mainly determined by surface

proton transmission. Using the Arrhenius equation to calculate its E_a being 0.15 eV, they think that its proton conduction obeys a Grotthuss mechanism.

In 2017, by employing a rigid triangulated phosphate ligand 2,4,6-tris(4-phosphonophenyl)pyridine (H$_6$FBTP), Z. H. Fard and co-workers solvothermally prepared a dense MOF, **(DMA)$_3$[Zr(HFBTP)F$_2$]** (DMA = dimethylammonium),[86] in which the ZrO$_4$F$_2$ octahedron and PO$_3$C tetrahedron are joined by organic ligands to build up a double-layer structure. The double-layer extends along the *a*-axis and stacks along the *c*-axis in AAA sequence. AC impedance determinations showed that the σ value of **(DMA)$_3$[Zr(HFBTP)F$_2$]** had a certain dependence on temperature, reaching a maximum value of 1×10^{-2} S cm^{-1} at 80 °C and 95% RH. Note that the initial σ value of this MOF is about 10^{-5} S cm^{-1} under 20 °C and 95% RH. Continuous heating/cooling cycles indicated that the σ value of this MOF only can be 3×10^{-3} S cm^{-1} under the same conditions, which never get back to the original number of 10^{-5} S cm^{-1}. Thus, the researchers suggested that the phase change happened to this MOF from 20–70 °C and the phase was named **PCMOF20**. To study **PCMOF20** more deeply, the authors re-prepared **PCMOF20**, and found that **PCMOF20** has higher porosity, thermal stability and water stability. In addition, the structure of **PCMOF20** had been determined, whose coordination environment is similar to **(DMA)$_3$[Zr(HFBTP)F$_2$]**, and the distance and direction of aromatic hydrocarbons changed relative to **(DMA)$_3$[Zr(HFBTP)F$_2$]**. The migration of protons in **PCMOF20** is highly dependent on water molecules, and there is almost no conductivity under anhydrous conditions, but the proton conductivity will increase with increasing humidity. The ultrahigh proton conductivity and stability of **PCMOF20** indicate that it has great application prospects in the field of fuel cells.

Recently, K. Melánová *et al.*[87] successfully prepared a series of mixed phosphate organophosphonate MOFs, Zr(PO$_4$)(H$_2$PO$_4$)$_{1-2x}$(H$_2$TDP)$_x$·*y*H$_2$O (x = 0.15, 0.34, 0.45; y = 2, 1.5) by controlling the γ-ZrP/H$_4$TDP reaction ratio (γ-ZrP denotes the γ-modification compound Zr(PO$_4$)(H$_2$PO$_4$)·2H$_2$O, which was synthesized by a previous literature method;[88] H$_4$TDP = 2-bis(phosphonomethyl)amino-ethan-1-sulfonic acid). The layered structure of γ-ZrP includes ZrO$_6$ octahedra placed in two different planes and connected to each other with a tetradentate PO$_4$ inside and H$_2$PO$_4$ units outside these planes. For the parent γ-ZrP, the σ value is derived from the hydrogen bonding network formed by the interlayer H$_2$O units and the OH units of the external H$_2$PO$_4^-$ group. As the H$_2$TDP^{2-} units replaced some of the H$_2$PO$_4^-$ units, the hydrogen bonding network was damaged, and at the same time, the mobility of protons between the layers increased, resulting in an increase in σ values. When x is equal to 0.15, the proton conductivity of Zr(PO$_4$)(H$_2$PO$_4$)$_{0.70}$(H$_2$TDP)$_{0.15}$·2H$_2$O is the highest. In contrast, if the H$_2$PO$_4^-$ units are continually replaced, its proton conductivity will decrease, because the concentration and fluidity of unstable protons will decrease at this time. Overall, this series of MOFs shows negligible proton conductivity of about 10^{-5} S cm^{-1}.

This journal is © the Partner Organisations 2020

Inorg. Chem. Front., 2020, **7**, 3765–3784 | **3779**

Scheme 5 The organic linkages used in phenolic hydroxyl-based Zr-MOFs.

2.5. Phenolic hydroxyl group-based MOFs

Up to now, there are few reports on Zr-MOFs constructed from phenolic hydroxyl ligands (Scheme 5) in the literature, but these compounds often show super high structural stability, which is very helpful for conducting proton research.

In 2016, P. G. M. Mileo *et al.* synthesized [{$Zr_2(H_2$-$TzGal)_2$}·$(solvent)_n$, solvent = DMA and H_2O, H_6TzGal = 5,5′-(1,2,4,5-tetrazine-3,6-diyl)bis(benzene-1,2,3-triol)] (denoted as **MIL-163**) according to the reported method,[89] and explored its proton conductivity by experimental-modeling methods.[90] MIL-163 is a 3D open structure with square channels (aperture = 12 Å). Each Zr^{4+} ion is coordinated with eight oxygen atoms from four different H_2TzGal^{4-} anions to form a ZrO_8 polyhedron with shared edges, and these polyhedra extend along the c-axis into the ZrO_8 chain. These chains are further connected by H_2TzGal^{4-} anions to build up a 3D structure. The proton conductivity of **MIL-163** is very low under anhydrous conditions, which may be due to the lack of a conductive medium and the ineffective conduction of charge carriers. After increasing the humidity, the proton conductivity has been greatly improved, reaching the maximum value of 2.1×10^{-3} S cm^{-1} at 90 °C and 95% RH, indicating that the σ value of this MOF has a strong dependence on RH. In addition, the E_a value of **MIL-163** is 0.25 eV. Monte Carlo simulation of **MIL-163** found that a 3D H-bonding network can be formed inside the square channels, thereby generating multiple proton transport pathways, offering the best solution for the H_2O-mediated proton transport provided by phenol in the organic linker. At the same time, guest DMA units tend to form a H-bonded network with H_2O units inside the channels. These all contribute to the transport of protons, so **MIL-163** has good proton conductivity.

In 2017, E.-X. Chen *et al.*[91] reported two MOFs, $Zr_2(THPP)·(solvent)$ (namely **ZrPP-1**) and $Zr_2(THBPP)·(solvent)$ (namely **ZrPP-2**) (THPP = 5,10,15,20-tetrakis-(3,4,5-trihydroxyphenyl)porphyrin, THBPP = 5,10,15,20-tetrakis(3,4,5-trihydroxybiphenyl)porphyrin, and solvent = $NH(Me)_2$ and H_2O. The structures of the two MOFs are three-dimensional frameworks with nbo topology. Zr^{IV}-pyrogallate chains are running along the c-direction. Moreover, these rod-like chains are connected across porphyrinic spacers forming an nbo-type bearing elliptical pores (aperture ≈8 × 4 Å^2). The two MOFs have good chemical stability and can resist the contact of wet and even saturated NaOH aqueous solution. The σ value of the two MOFs

was determined at various temperatures and humidity. The results showed that the σ value increased with the increase of humidity, attaining the best value at 25 °C and 98% RH (for **ZrPP-1**: σ = 8.0×10^{-3} S cm^{-1}; for **ZrPP-2**: σ = 4.2×10^{-3} S cm^{-1}). Note that their good proton conductivity can be repeated at least in two successive measurements without significant changes. The high σ value of the two MOFs may be due to the existence of a large number of proton sources, such as acidic groups –OH, dimethylamine cations, and lattice water molecules. In addition, the calculated E_a values of MOFs are less than 0.40 eV (**ZrPP-1** and **ZrPP-2** being 0.21 and 0.23 eV, respectively) demonstrating a proton conducting Grotthuss mechanism.

In conclusion, the remarkable stability and high proton conductivity demonstrated by such compounds suggest their great promise in the field of proton conductivity.

3. Conclusions

Recently, a great deal of work have been carried out on the proton conductivity of crystalline MOF materials, but some of the shortcomings of MOFs, such as low stability and unstable bonding, have led to the bottleneck of the research. Therefore, zirconium-based MOFs with high structural stability, such as super water stability, high acid–base tolerance and high thermal stability, have attracted much attention. In this review, we classify and summarize Zr-based MOFs according to the type of organic ligand used (aromatic carboxylic acid, fatty carboxylic acid, phosphoric acid, sulfonic acid, *etc.*). Their structural characteristics, synthesis strategies, structural stability, and proton conductivity characteristics, especially the conductive mechanism, are summarized and discussed in detail. Hopefully, this review will help researchers to have a comprehensive understanding of the latest developments in proton conducting zirconium MOFs. For future research, we have the following suggestions: first, people should choose as many kinds of organic ligands as possible (such as asymmetric carboxylic acids, ferrocene-based carboxylic acids, *etc.*) to construct more Zr-MOFs, so as to facilitate the research of proton conductivity. Second, so far, there are few studies on proton conductivity using single crystal Zr-MOFs, which limits the in-depth understanding of the conduction mechanism. It is hoped that more single crystal products can be obtained for proton conduction research in the next step. Third, it is hoped that more Zr-MOFs can be applied to composite membranes and fuel cells to study their application values. In a word, Zr-MOFs are promising proton conducting crystalline materials with great application prospects, which are worthy of further study.

Conflicts of interest

There are no conflicts to declare.

Acknowledgements

References

1 V. F. Valdes-Lopez, T. Mason, P. R. Shearing and D. J. L. Brett, Carbon monoxide poisoning and mitigation strategies for polymer electrolyte membrane fuel cells - A review, *Prog. Energy Combust. Sci.*, 2020, **79**, 100842.

2 M. Shabani, H. Younesi, M. Pontie, A. Rahimpour, M. Rahimnejad and A. A. Zinatizadeh, A critical review on recent proton exchange membranes applied in microbial fuel cells for renewable energy recovery, *J. Cleaner Prod.*, 2020, **264**, 121446.

3 R. S. R. Rafidah, W. Rashmi, M. Khalid, W. Y. Wong and J. Priyanka, Recent progress in the development of aromatic polymer-based proton exchange membranes for fuel cell applications, *Polymers*, 2020, **12**, 1061.

4 M. Fang, C. Montoro and M. Semsarilar, Metal and covalent organic frameworks for membrane applications, *Membranes*, 2020, **10**, 107.

5 D. W. Kang, M. Kang and C. S. Hong, Post-synthetic modification of porous materials: superprotonic conductivities and membrane applications in fuel cells, *J. Mater. Chem. A*, 2020, **8**, 7474–7494.

6 L. Zanchet, L. G. da Trindade, W. Bariviera, K. M. N. Borba, R. D. M. Santos, V. A. Paganin, C. P. de Oliveira, E. A. Ticianelli, E. M. A. Martini and M. O. de Souza, 3-Triethylammonium propane sulfonate ionic liquids for Nafion-based composite membranes for PEM fuel cells, *J. Mater. Sci.*, 2020, **55**, 11794–11795.

7 K. A. Mauritz and R. B. Moore, State of understanding of Nafion, *Chem. Rev.*, 2004, **104**, 4535–4586.

8 X. Liang, K. Cai, F. Zhang, J. Liu and G. Zhu, A proton-conductive lanthanide oxalatophosphonate framework featuring unique chemical stability: stabilities of bulk phase and surface structure, *J. Mater. Chem. A*, 2017, **5**, 25350–25358.

9 X.-X. Xie, Z. Zhang, J. Zhang, L. Hou, Z. Li and G. Li, Impressive proton conductivities of two highly stable metal-organic frameworks constructed by substituted imidazole dicarboxylates, *Inorg. Chem.*, 2019, **58**, 5173–5182.

10 X.-L. Sun, W.-H. Deng, H. Chen, H.-L. Han, J. M. Taylor, C.-Q. Wan and G. Xu, A metal–organic framework impregnated with a binary ionic liquid for safe proton conduction above 100 °C, *Chem. – Eur. J.*, 2017, **23**, 1248–1252.

11 Z. Sun, S. Yu, L. Zhao, J. Wang, Z. Li and G. Li, A highly stable two-dimensional copper(II)-organic framework for proton conduction and ammonia impedance sensing, *Chem. – Eur. J.*, 2018, **24**, 10829–10839.

12 T. He, Y.-Z. Zhang, H. Wu, X.-J. Kong, X.-M. Liu, L.-H. Xie, Y. Dou and J.-R. Li, Functionalized base-stable metal–organic frameworks for selective CO_2 adsorption and proton conduction, *ChemPhysChem*, 2017, **18**, 3245–3252.

13 D. Gui, X. Dai, Z. Tao, T. Zheng, X. Wang, M. A. Silver, J. Shu, L. Chen, Y. Wang, T. Zhang, J. Xie, L. Zou, Y. Xia, J. Zhang, J. Zhang, L. Zhao, J. Diwu, R. Zhou, Z. Chai and S. Wang, Unique proton transportation pathway in a robust inorganic coordination polymer leading to intrinsically high and sustainable anhydrous proton conductivity, *J. Am. Chem. Soc.*, 2018, **140**, 6146–6155.

14 S. M. Elahi, S. Chand, W.-H. Deng, A. Pal and M. C. Das, Polycarboxylate-templated coordination polymers: role of templates for superprotonic conductivities of up to 10^{-1} Scm^{-1}, *Angew. Chem.*, 2018, **130**, 6772–6776.

15 H. Chen, S.-Y. Han, R.-H. Liu, T.-F. Chen, K.-L. Bi, J.-B. Liang, Y.-H. Deng and C.-Q. Wan, High conductive, long-term durable, anhydrous proton conductive solid-state electrolyte based on a metal-organic framework impregnated with binary ionic liquids: Synthesis, characteristic and effect of anion, *J. Power Sources*, 2018, **376**, 168–176.

16 W.-H. Xing, H.-Y. Li, X.-Y. Dong and S.-Q. Zang, Robust multifunctional Zr-based metal–organic polyhedra for high proton conductivity and selective CO_2 capture, *J. Mater. Chem. A*, 2018, **6**, 7724–7730.

17 H. Zhong, Z.-H. Fu, J. M. Taylor, G. Xu and R.-H. Wang, Inorganic acid-impregnated covalent organic gels as high-performance proton-conductive materials at subzero temperatures, *Adv. Funct. Mater.*, 2017, **27**, 1701465.

18 X. Liang, B. Li, M. Wang, J. Wang, R. Liu and G. Li, Effective approach to promoting the proton conductivity of metal−organic frameworks by exposure to aqua−ammonia vapor, *ACS Appl. Mater. Interfaces*, 2017, **9**, 25082–25086.

19 F. Guo, C. Chen, K. Wang, Q. Zhang and Z. Lin, Supramolecular templating approach for the solvent-free synthesis of open-framework metal oxalates, *Inorg. Chem.*, 2016, **55**, 7817–7819.

20 R. Liu, L. Zhao, W. Dai, C. Yang, X. Liang and G. Li, A comparative investigation on proton conductivities for two metal-organic frameworks under water and aqua-ammonia vapors, *Inorg. Chem.*, 2018, **57**, 1474–1482.

21 S. Chand, S. M. Elahi, A. Pal and M. C. Das, Metal–organic frameworks and other crystalline materials for ultrahigh superprotonic conductivities of 10^{-2} Scm^{-1} or Higher, *Chem. – Eur. J.*, 2019, **25**, 6259–6269.

22 Z.-C. Guo, Z.-Q. Shi, X.-Y. Wang, Z.-F. Li and G. Li, Proton conductive covalent organic frameworks, *Coord. Chem. Rev.*, 2020, **422**, 213465.

23 T. Jadhav, Y. Fang, C.-H. Liu, A. Dadvand, E. Hamzehpoor, W. Patterson, A. Jonderian, R. S. Stein and D. F. Perepichka, Transformation between 2D and 3D covalent organic frameworks via reversible [2+2] cycloaddition, *J. Am. Chem. Soc.*, 2020, **142**, 8862–8870.

24 B. Zhou, J. Le, Z. Cheng, X. Zhao, M. Shen, M. Xie, B. Hu, X. Yang, L. Chen and H. Chen, Simple transformation of covalent organic frameworks to highly proton-conductive electrolytes, *ACS Appl. Mater. Interfaces*, 2020, **12**, 8198–8205.

This journal is © the Partner Organisations 2020

Inorg. Chem. Front., 2020, **7**, 3765–3784 | **3781**

25 A. Karmakar, R. Illathvalappil, B. Anothumakkool, A. Sen, P. Samanta, A. V. Desai, S. Kurungot and S. K. Ghosh, Hydrogen-bonded organic frameworks (HOFs): a new class of porous crystalline proton-conducting materials, *Angew. Chem., Int. Ed.*, 2016, **55**, 10667–10671.

26 Z.-B. Sun, Y.-L. Li, Z.-H. Zhang, Z.-F. Li, B. Xiao and G. Li, A path to improve proton conductivity: from a 3D hydrogen-bonded organic framework to a 3D copper-organic framework, *New J. Chem.*, 2019, **43**, 10637–10644.

27 W. Yang, F. Yang, T.-L. Hu, S.-C. King, H. Wang, H. Wu, W. Zhou, J.-R. Li, H. D. Arman and B. L. Chen, Microporous diaminotriazine-decorated porphyrin-based hydrogen bonded organic framework: permanent porosity and proton conduction, *Cryst. Growth Des.*, 2016, **16**, 5831–5835.

28 Y. Qin, T.-L. Gao, W.-P. Xie, Z.-F. Li and G. Li, Ultrahigh proton conduction in two highly stable ferrocenyl carboxylate frameworks, *ACS Appl. Mater. Interfaces*, 2019, **11**, 31018–31027.

29 Z.-Q. Shi, N.-N. Ji, M.-H. Wang and G. Li, A comparative study of proton conduction between a 2D Zinc(II) MOF and its corresponding organic ligand, *Inorg. Chem.*, 2020, **59**, 4781–4789.

30 Y. Qin, X. Wang, W. Xie, Z. Li and G. Li, Structural effect on proton conduction in two highly stable disubstituted ferrocenyl carboxylate frameworks, *Inorg. Chem.*, 2020, **59**, 10243–10252.

31 S. Kanda, K. Yamashita and K. Ohkawa, A proton conductive coordination polymer. I. [N,N′-bis(2-hydroxyethyl) dithiooxamido]copper(II), *Bull. Chem. Soc. Jpn.*, 1979, **52**, 3296–3301.

32 S.-S. Bao, G. K. H. Shimizu and L.-M. Zheng, Proton conductive metal phosphonate frameworks, *Coord. Chem. Rev.*, 2019, **378**, 577–594.

33 X.-X. Xie, Y.-C. Yang, B.-H. Dou, Z.-F. Li and G. Li, Proton conductive carboxylate-based metal-organic frameworks, *Coord. Chem. Rev.*, 2020, **403**, 213100.

34 W.-H. Li, W.-H. Deng, G.-E. Wang and G. Xu, Conductive MOFs, *EnergyChem*, 2020, **2**, 100029.

35 J. Ha, J. Hwa Lee and H. Moon, Alterations to secondary building units of metal–organic frameworks for the development of new functions, *Inorg. Chem. Front.*, 2020, **7**, 12–27.

36 H.-N. Wang, X. Meng, L.-Z. Dong, Y. Chen, S.-L. Li and Y.-Q. Lan, Coordination polymer-based conductive materials: ionic conductivity vs. electronic conductivity, *J. Mater. Chem. A*, 2019, **7**, 24059–24091.

37 D. W. Lim, M. Sadakiyo and H. Kitagawa, Proton transfer in hydrogen-bonded degenerate systems of water and ammonia in metal–organic frameworks, *Chem. Sci.*, 2019, **10**, 16–33.

38 Y. Ye, L. Gong, S. Xiang, Z. Zhang and B. Chen, Metal–organic frameworks as a versatile platform for proton conductors, *Adv. Mater.*, 2020, **32**, 1907090.

39 X. Meng, H.-N. Wang, S.-Y. Song and H.-J. Zhang, Proton-conducting crystalline porous materials, *Chem. Soc. Rev.*, 2017, **46**, 464–480.

40 J. H. Cavka, S. Jakobsen, U. Olsbye, N. Guillou, C. Lamberti, S. Bordiga and K. P. Lillerud, A new zirconium inorganic building brick forming metal organic frameworks with exceptional stability, *J. Am. Chem. Soc.*, 2008, **130**, 13850–13851.

41 Y. Bai, Y. Dou, L.-H. Xie, W. Rutledge, J.-R. Li and H.-C. Zhou, Zr-based metal–organic frameworks: design, synthesis, structure, and applications, *Chem. Soc. Rev.*, 2016, **45**, 2327–2367.

42 D. R. Sun and Z. H. Li, Robust Ti- and Zr-based metal-organic frameworks for photocatalysis, *Chin. J. Chem.*, 2017, **35**, 135–147.

43 T. N. Tu, M. V. Nguyen, H. L. Nguyen, B. Yuliarto, K. E. Cordova and S. Demir, Designing bipyridine-functionalized zirconium metal-organic frameworks as a platform for clean energy and other emerging applications, *Coord. Chem. Rev.*, 2018, **364**, 33–50.

44 J. M. Taylor, S. Dekura, R. Ikeda and H. Kitagawa, Defect control to enhance proton conductivity in a metal–organic framework, *Chem. Mater.*, 2015, **27**, 2286–2289.

45 J. M. Taylor, T. Komatsu, S. Dekura, K. Otsubo, M. Takata and H. Kitagawa, The role of a three dimensionally ordered defect sublattice on the acidity of a sulfonated metal–organic framework, *J. Am. Chem. Soc.*, 2015, **137**, 11498–11506.

46 S. Biswas, J. Zhang, Z. Li, Y.-Y. Liu, M. Grzywa, L. Sun, D. Volkmer and P. V. D. Voort, Enhanced selectivity of CO_2 over CH4 in sulphonate-, carboxylate- and iodo-functionalized UiO-66 frameworks, *Dalton Trans.*, 2013, **42**, 4730–4737.

47 Q. Yang, S. Vaesen, F. Ragon, A. D. Wiersum, D. Wu, A. Lago, T. Devic, C. Martineau, F. Taulelle, P. L. Llewellyn, H. Jobic, C. Zhong, C. Serre, G. D. Weireld and G. Maurin, A water stable metal–organic framework with optimal features for CO_2 capture, *Angew. Chem.*, 2013, **125**, 10506–10510.

48 M. J. Katz, Z. J. Brown, Y. J. Colón, P. W. Siu, K. A. Scheidt, R. Q. Snurr, J. T. Hupp and O. K. Farha, A facile synthesis of UiO-66, UiO-67 and their derivatives, *Chem. Commun.*, 2013, **49**, 9449–9451.

49 W. Zhang, H. Huang, C. Zhong and D. Liu, Cooperative effect of temperature and linker functionality on CO_2 capture from industrial gas mixtures in metal–organic frameworks: a combined experimental and molecular simulation study, *Phys. Chem. Chem. Phys.*, 2012, **14**, 2317–2325.

50 F. Yang, H. Huang, X. Wang, F. Li, Y. Gong, C. Zhong and J.-R. Li, Proton conductivities in functionalized UiO-66: tuned properties, thermogravimetry mass, and molecular simulation analyses, *Cryst. Growth Des.*, 2015, **15**, 5827–5833.

51 W. J. Phang, H. Jo, W. R. Lee, J. H. Song, K. Yoo, B. Kim and C. S. Hong, Superprotonic conductivity of a UiO-66 framework functionalized with sulfonic acid groups by facile postsynthetic oxidation, *Angew. Chem., Int. Ed.*, 2015, **54**, 5142–5146.

3782 | *Inorg. Chem. Front.*, 2020, **7**, 3765–3784

This journal is © the Partner Organisations 2020

52 S. Balčiunas, D. Pavlovaitè, M. Kinka, J. Y. Yeh, P. C. Han, F. K. Shieh, K. C. W. Wu, M. Šimènas, R. Grigalaitis and J. Banys, Dielectric spectroscopy of water dynamics in functionalized UiO-66 metal-organic frameworks, *Molecules*, 2020, **25**, 1962.

53 S. Mukhopadhyay, J. Debgupta, C. Singh, R. Sarkar, O. Basu and S. K. Das, Designing UiO-66-based superprotonic conductor with the highest metal−organic framework based proton conductivity, *ACS Appl. Mater. Interfaces*, 2019, **11**, 13423–13432.

54 X.-M. Li, J. Liu, C. Zhao, J.-L. Zhou, L. Zhao, S.-L. Li and Y.-Q. Lan, Strategic hierarchical improvement of superprotonic conductivity in a stable metal–organic framework system, *J. Mater. Chem. A*, 2019, **7**, 25165–25171.

55 A. Planchais, S. Devautour-Vinot, F. Salles, F. Ragon, T. Devic, C. Serre and G. Maurin, A joint experimental/computational exploration of the dynamics of confined water/Zr-based MOFs systems, *J. Phys. Chem. C*, 2014, **118**, 14441–14448.

56 D. D. Borges, S. Devautour-Vinot, H. Jobic, J. Ollivier, F. Nouar, R. Semino, T. Devic, C. Serre, F. Paesani and G. Maurin, Proton transport in a highly conductive porous zirconium-based metal–organic framework: molecular insight, *Angew. Chem., Int. Ed.*, 2016, **55**, 3919–3924.

57 R. Zhuang, B.-B. Tang and P.-Y. Wu, Proton conductivity of proton exchange membrane synergistically promoted by different functionalized Metal-Organic Frameworks, *ACS Appl. Mater. Interfaces*, 2017, **9**, 22597–22603.

58 X.-Y. Dong, J.-H. Wang, S.-S. Liu, Z. Han, Q.-J. Tang, F.-F. Li and S.-Q. Zang, Synergy between isomorphous acid and basic metal-organic frameworks for anhydrous proton conduction of low-cost hybrid membranes at high temperatures, *ACS Appl. Mater. Interfaces*, 2018, **10**, 38209–38216.

59 Z. Rao, K. Feng, B.-B. Tang and P.-Y. Wu, Construction of well interconnected metal-organic framework structure for effectively promoting proton conductivity of proton exchange membrane, *J. Membr. Sci.*, 2017, **533**, 160–170.

60 P.-L. Zheng, Q.-Y. Liu, D.-H. Wang, Z.-K. Li, Y.-W. Meng and Y. Zheng, Preparation of covalent-ionically cross-linked UiO-66-NH$_2$/sulfonated aromatic composite proton exchange membranes with excellent performance, *Front. Chem.*, 2020, **8**, 56.

61 L. Wang, N. Deng, Y. Liang, J. Ju, B. Cheng and W. Kang, Metal-organic framework anchored sulfonated poly(ether sulfone) nanofibers as highly conductive channels for hybrid proton exchange membranes, *J. Power Sources*, 2020, **450**, 227592.

62 H.-Z. Sun, B.-B. Tang and P.-Y. Wu, Rational design of S–UiO-66@GO hybrid nanosheets for proton exchange membranes with significantly enhanced transport performance, *ACS Appl. Mater. Interfaces*, 2017, **9**, 26077–26087.

63 A. Donnadio, R. Narducci, M. Casciola, F. Marmottini, R. D'Amato, M. Jazestani, H. Chiniforoshan and F. Costantino, Mixed membrane matrices based on Nafion/UiO-66/SO$_3$H–UiO-66 nano-MOFs: revealing the effect of crystal size, sulfonation, and filler loading on the mechani-

cal and conductivity properties, *ACS Appl. Mater. Interfaces*, 2017, **9**, 42239–42246.

64 S. Neelakandan, R. Ramachandran, M. Fang and L. Wang, Improving the performance of sulfonated polymer membrane by using sulfonic acid functionalized heterometallic metal-organic framework for DMFC applications, *Int. J. Energy Res.*, 2020, **44**, 1673–1684.

65 S. Liu, Z. Yue and Y. Liu, Incorporation of imidazole within the metal–organic framework UiO-67 for enhanced anhydrous proton conductivity, *Dalton Trans.*, 2015, **44**, 12976–12980.

66 W.-R. Xian, Y. He, Y. Diao, Y.-L. Wong, H.-Q. Zhou, S.-L. Zheng, W.-M. Liao, Z. Xu and J. He, A bumper crop of boiling-water-stable metal–organic frameworks from controlled linker sulfuration, *Inorg. Chem.*, 2020, **59**, 7097–7102.

67 H. Furukawa, F. Gandara, Y. B. Zhang, J. Jiang, W. L. Queen, M. R. Hudson and O. M. Yaghi, Water adsorption in porous metal−organic frameworks and related materials, *J. Am. Chem. Soc.*, 2014, **136**, 4369–4381.

68 H.-B. Luo, M. Wang, S.-X. Liu, C. Xue, Z.-F. Tian, Y. Zou and X.-M. Ren, Proton conductance of a superior water-stable metal–organic framework and its composite membrane with poly(vinylidenefluoride), *Inorg. Chem.*, 2017, **56**, 4169–4175.

69 X. Meng, H.-N. Wang, L.-S. Wang, Y.-H. Zou and Z.-Y. Zhou, Enhanced proton conductivity of a MOF-808 framework through anchoring organic acids to the zirconium clusters by post-synthetic modification, *CrystEngComm*, 2019, **21**, 3146–3150.

70 H. A. Patel, N. Mansor, S. Gadipelli, D. J. L. Brett and Z. Guo, Superacidity in Nafion/MOF hybrid membranes retains water at low humidity to enhance proton conduction for fuel cells, *ACS Appl. Mater. Interfaces*, 2016, **8**, 30687–30691.

71 J.-C. Jiang, F. Gandara, Y.-B. Zhang, K. Na, O. M. Yaghi and W. G. Klemperer, Superacidity in sulfated metal-organic framework-808, *J. Am. Chem. Soc.*, 2014, **136**, 12844–12847.

72 T. H. N. Lo, M. V. Nguyen and T. N. Tu, An anchoring strategy leads to enhanced proton conductivity in a new metal–organic framework, *Inorg. Chem. Front.*, 2017, **4**, 1509–1516.

73 M. V. Nguyen, T. H. N. Lo, L. C. Luu, H. T. T. Nguyen and T. N. Tu, Enhancing proton conductivity in a metal–organic framework at T > 80 °C by an anchoring strategy, *J. Mater. Chem. A*, 2018, **6**, 1816–1821.

74 Q. Zeng, W.-R. Xian, Y.-H. Zhong, L.-H. Chung, W.-M. Liao and J. He, Highly enhanced hydrated proton conductivity by combination of post-synthetic oxidation and acidification in a zirconium-organic framework, *J. Solid State Chem.*, 2020, **285**, 121234.

75 S. Tominaka, F. Coudert, T. D. Dao, T. Nagao and A. K. Cheetham, Insulator-to-proton-conductor transition in a dense metal–organic framework, *J. Am. Chem. Soc.*, 2015, **137**, 6428–6431.

76 S.-J. Wang, M. Wahiduzzaman, L. Davis, A. Tissot, W. Shepard, J. Marrot, C. Martineau-Corcos, D. Hamdane, G. Maurin, S. Devautour-Vinot and C. Serre, A robust zirco-

This journal is © the Partner Organisations 2020

Inorg. Chem. Front., 2020, **7**, 3765–3784 | **3783**

nium amino acid metal-organic framework for proton conduction, *Nat. Commun.*, 2018, **9**, 4937.

77 J. Zhang, H.-J. Bai, Q. Ren, H.-B. Luo, X.-M. Ren, Z.-F. Tian and S.-F. Lu, Extra water- and acid-stable MOF-801 with high proton conductivity and its composite membrane for proton-exchange membrane, *ACS Appl. Mater. Interfaces*, 2018, **10**, 28656–28663.

78 Z. Zhang, J. Ren, J. Xu, Z. Wang, W. He, S. Wang, X. Yang, X. Du, L. Meng and P. Zhao, Adjust the arrangement of imidazole on the metal-organic framework to obtain hybrid proton exchange membrane with long-term stable high proton conductivity, *J. Membr. Sci.*, 2020, **607**, 118194.

79 G. Alberti, M. Casciola, A. Donnadio, P. Piaggio, M. Pica and M. Sisani, Preparation and characterisation of a-layered zirconium phosphate sulfophenylenphosphonates with variable concentration of sulfonic groups, *Solid State Ionics*, 2005, **176**, 2893–2898.

80 Z. Li, F. Dong, L. Xu, S. Wang and X. Yu, Preparation and properties of medium temperature membranes based on zirconium sulfophenylphosphate/sulfonated poly(phthalazinone ether sulfone ketone) for direct methanol fuel cells, *J. Membr. Sci.*, 2010, **351**, 50–57.

81 E. W. Stein, S. A. Clearfield and M. A. Subramanianm, Conductivity of group IV metal sulfophosphonates and a new class of interstratified metal amine-sulfophosphonates, *Solid State Ionics*, 1996, **83**, 113–124.

82 V. Zima, J. Svoboda, K. Melánová, L. Beneš, M. Casciola, M. Sganappa, J. Brus and M. Trchová, Synthesis and characterization of new zirconium 4-sulfophenylphosphonates, *Solid State Ionics*, 2010, **18**, 705–713.

83 F. Costantino, A. Donnadio and M. Casciola, Survey on the phase transitions and their effect on the ion-exchange and on the proton-conduction properties of a flexible and robust zr phosphonate coordination polymer, *Inorg. Chem.*, 2012, **51**, 6992–7000.

84 M. Taddei, A. Donnadio, F. Costantino, R. Vivani and M. Casciola, Synthesis, crystal structure, and proton conductivity of one-dimensional, two-dimensional, and three-dimensional zirconium phosphonates based on glyphosate and glyphosine, *Inorg. Chem.*, 2013, **52**, 12131–12139.

85 A. Donnadio, M. Nocchetti, F. Costantino, M. Taddei, M. Casciola, F. da Silva Lisboa and R. Vivani, A layered mixed zirconium phosphate/phosphonate with exposed carboxylic and phosphonic groups: x-ray powder structure and proton conductivity properties, *Inorg. Chem.*, 2014, **53**, 13220–13226.

86 Z. H. Fard, N. E. Wong, C. D. Malliakas, P. Ramaswamy, J. M. Taylor, K. Otsubo and G. K. H. Shimizu, Superprotonic phase change to a robust phosphonate metal−organic framework, *Chem. Mater.*, 2018, **30**, 314–318.

87 K. Melánová, J. Brus, V. Zima, L. Beneš, J. Svoboda, L. Kobera and P. Kutálek, Formation of layered proton-conducting zirconium and titanium organophosphonates by topotactic reaction: physicochemical properties, proton dynamics, and atomic-resolution structure, *Inorg. Chem.*, 2020, **59**, 505–513.

88 D. M. Poojary, B. Shpeizer and A. Clearfield, X-ray powder structure and rietveld refinement of gamma-zirconium phosphate, $Zr(PO_4)(H_2PO_4) \cdot 2H_2O$, *J. Chem. Soc., Dalton Trans.*, 1995, 111–113.

89 G. Mouchaham, L. Cooper, N. Guillou, C. Martineau, E. Elkaïm, S. Bourrelly, P. L. Llewellyn, C. Allain, G. Clavier, C. Serre and T. Devic, A robust infinite zirconium phenolate building unit to enhance the chemical stability of Zr MOFs, *Angew. Chem., Int. Ed.*, 2015, **54**, 13297–13301.

90 P. G. M. Mileo, S. Devautour-Vinot, G. Mouchaham, F. Faucher, N. Guillou, A. Vimont, C. Serre and G. Maurin, Proton-conducting phenolate-based Zr metal−organic framework: a joint experimental−modeling investigation, *J. Phys. Chem. C*, 2016, **120**, 24503–24510.

91 E.-X. Chen, G. Xu and Q. Lin, Robust porphyrin-spaced zirconium pyrogallate frameworks with high proton conduction, *Inorg. Chem.*, 2019, **58**, 3569–3573.